

Correlation functions in liquids and crystals: Free-energy functional and liquid-to-crystal transitionAtul S. Bharadwaj, Swarn L. Singh,^{*} and Yashwant Singh*Department of Physics, Banaras Hindu University, Varanasi 221 005, India*

(Received 29 March 2013; published 9 August 2013)

A free-energy functional for a crystal that contains both the symmetry-conserved and symmetry-broken parts of the direct pair-correlation function has been used to investigate the crystallization of fluids in three dimensions. The symmetry-broken part of the direct pair-correlation function has been calculated using a series in ascending powers of the order parameters and which contains three- and higher-body direct correlation functions of the isotropic phase. It is shown that a very accurate description of freezing transitions for a wide class of potentials is found by considering the first two terms of this series. The results found for freezing parameters including the structure of the frozen phase for fluids interacting via the inverse power potential $u(r) = \epsilon (\sigma/r)^n$ for n ranging from 4 to ∞ are in very good agreement with simulation results. It is found that for $n > 6.5$ the fluid freezes into a face-centered cubic (fcc) structure while for $n \leq 6$ the body-centered cubic (bcc) structure is preferred. The fluid-bcc-fcc triple point is found to be at $1/n = 0.158$, which is in good agreement with simulation result.

DOI: [10.1103/PhysRevE.88.022112](https://doi.org/10.1103/PhysRevE.88.022112)

PACS number(s): 05.70.Fh, 64.70.D-, 64.70.pm

I. INTRODUCTION

Freezing of a fluid into a crystalline solid is a particular, but important, example of a first-order phase transition in which the continuous symmetry of the fluid is broken into one of the Bravais lattices. The transition in three dimensions is marked by large discontinuities in entropy, density, and order parameters, the order parameters being proportional to the lattice components of one particle density distribution $\rho(\vec{r})$ [see Eq. (2.3)]. Efforts have been made for over six decades [1,2] to find a first-principles theory which can answer questions regarding at what density, pressure, and temperature does a particular fluid freeze? What is the change in entropy and the change in density upon freezing? Which of the Bravais lattices emerges at the freezing point for a given system and what are values of the order parameters?

A crystal is a system of extreme inhomogeneities where the value of $\rho(\vec{r})$ shows a several-orders-of-magnitude difference between its values on the lattice sites and in the interstitial regions. The density-functional formalism of classical statistical mechanics has been employed to develop theories for freezing transitions [2,3]. This kind of approach was initiated in 1979 by Ramakrishnan and Yussouff (RY) [4], which was later reformulated by Haymet and Oxtoby [5]. The central quantity in this formalism is the reduced Helmholtz free energy of both the crystal, $A[\rho]$, and the fluid, $A(\rho_l)$ [2]. For crystals, $A[\rho]$ is a unique functional of $\rho(\vec{r})$, whereas for fluids, $A(\rho_l)$ is simply a function of fluid density ρ_l which is a constant, independent of position.

The density-functional formalism is used to write an expression for $A[\rho]$ (or for the grand thermodynamic potential) in terms of $\rho(\vec{r})$ and the direct pair-correlation function (DPCF). Minimization of this expression with respect to $\rho(\vec{r})$ leads to an expression that relates $\rho(\vec{r})$ to the DPCF. The DPCF that appears in these equations corresponds to the crystal and

is functional of $\rho(\vec{r})$ and therefore depends on values of the order parameters. In the RY theory the functional dependence of the DPCF on $\rho(\vec{r})$ was neglected and was replaced by that of the coexisting fluid of density ρ_l . Attempts to improve the RY theory by incorporating a term involving three-body direct correlation function of the coexisting fluid in the expression of $A[\rho]$ have failed [6,7]. The efforts made by Tarazona [8], Curtin, Ashcraft, and Denton [9,10], and others [11,12] in the direction of developing a theory using what is referred to as the *weighted density approximation* have also met with only limited success.

The reason, as has been pointed out recently [13,14], is that at the fluid-solid transition the isotropy and the homogeneity of space is spontaneously broken and a qualitatively new contribution to the correlation in distribution of particles emerges. This fact has been used to write the DPCF of the frozen phase as a sum of two terms: one that preserves the continuous symmetry of the fluid and one that breaks it and vanishes in the fluid. An exact expression for the free-energy functional was found by performing double functional integration in density space of a relation that relates the second functional derivative of $A[\rho]$ with respect to $\rho(\vec{r})$ to the DPCF [see Eq. (2.7)]. This expression of free-energy functional contains both the symmetry-conserved and the symmetry-broken parts of the DPCF.

The values of the DPCF as well as of the total pair-correlation function (described in Sec. II) in a classical system can be found from solution of integral equation, the Ornstein-Zernike (OZ) equation, and a closure relation that relates correlation functions to pair potential [15]. The integral equation theory has been quite successful in getting values of pair-correlation functions of uniform fluids [15], but its application to find pair correlation functions of symmetry-broken phases has so far been limited. Recently, Mishra and Singh [16] have used the OZ equation and the Percus-Yevick (PY) closure relation to obtain both the symmetry-conserved and symmetry-broken parts of pair correlation functions in a nematic phase. In the nematic phase the orientational symmetry is broken but the translational symmetry of the fluid phase remains intact, whereas in a crystal both the orientational and the translational symmetries of the fluid phase are broken.

^{*}Present address: Max Planck Institute for Intelligent Systems, Heisenbergstr. 3, 70569 Stuttgart, Germany and Institut für Theoretische Physik IV, Universität Stuttgart, Pfaffenwaldring 57, 70569 Stuttgart, Germany.

Since closure relations are derived assuming translational invariance [15], they are valid in normal fluids as well as in nematics but may not be in crystals. In view of this, Singh and Singh [13] suggested a method in which the symmetry-broken part of the DPCF is expanded in ascending powers of order parameters. This series contains three- and higher-body direct correlation functions of the isotropic phase. The first term of this series was evaluated and used in investigating the freezing transitions in two and three dimensions of fluids interacting via inverse power potentials [13,17] and freezing of hard spheres into crystalline and glassy phases [14]. It has been found that contribution made by the symmetry-broken part to the grand thermodynamic potential at the freezing point increases with softness of the potential [13,17]. This suggests that for long-ranged potentials the higher-order terms of the series may not be negligible and need to be considered.

In this paper we calculate first and second terms of the series [see Eq. (2.29)] which involve three- and four-body direct correlation functions of the isotropic phase. We calculate the four-body direct correlation function by extending the method developed to calculate the three-body direct correlation function. The values found for the DPCF are used in the free-energy functional and the crystallization of fluids is investigated. We show that this free-energy functional gives a very accurate description of freezing transitions for a wide class of potentials.

The paper is organized as follows: In Sec. II we describe correlation functions in fluids and in crystals and calculate them. The symmetry-broken part of the DPCF is evaluated using first two terms of a series in ascending powers of order parameters. These results are used in the free-energy functional in Sec. III to calculate the contributions made by different parts of the DPCF to the grand thermodynamic potential at the freezing point. In Sec. IV we calculate these terms and locate the freezing points for fluids interacting via the inverse power potentials and compare our results with those found from computer simulations and from approximate free-energy functionals. The paper ends with a brief summary and perspectives given in Sec. V.

II. CORRELATION FUNCTIONS

The equilibrium one particle distribution $\rho(\vec{r})$ defined as

$$\rho(\vec{r}) = \left\langle \sum_l \delta(\vec{r} - \vec{r}_l) \right\rangle, \quad (2.1)$$

where \vec{r}_l is position vector of the l^{th} particle and the angular bracket $\langle \dots \rangle$ represents the ensemble average and is a constant, independent of position for a normal fluid but containing most of the structural informations of a crystal. For a crystalline solid there exists a discrete set of vectors \vec{R}_i such that

$$\rho(\vec{r}) = \rho(\vec{r} + \vec{R}_i), \quad \text{for all } \vec{R}_i. \quad (2.2)$$

This set of vectors which appears at the freezing point due to spontaneous breaking of continuous symmetry of a fluid necessarily forms a Bravais lattice. The $\rho(\vec{r})$ in a crystal can be written as a sum of two terms:

$$\rho(\vec{r}) = \rho_0 + \rho^{(b)}(\vec{r}), \quad (2.3a)$$

where

$$\rho^{(b)}(\vec{r}) = \sum_G \rho_G e^{i\vec{G}\cdot\vec{r}}. \quad (2.3b)$$

Here ρ_0 is the average density of the crystal and ρ_G are the order parameters (amplitude of density waves of wavelength $2\pi/|\vec{G}|$). The sum in Eq. (2.3b) is over a complete set of reciprocal lattice vectors (RLV) \vec{G} with the property that $e^{i\vec{G}\cdot\vec{R}_i} = 1$ for all \vec{G} and for all \vec{R}_i . We refer the first term of Eq. (2.3a) as symmetry conserved and the second as symmetry-broken parts of single-particle distribution $\rho(\vec{r})$.

The two-particle density distribution $\rho^{(2)}(\vec{r}_1, \vec{r}_2)$ which gives probability of finding simultaneously a particle in volume element $d\vec{r}_1$ at \vec{r}_1 and a second particle in volume element $d\vec{r}_2$ at \vec{r}_2 , is defined as

$$\rho^{(2)}(\vec{r}_1, \vec{r}_2) = \left\langle \sum_j \sum_{k \neq j} \delta(\vec{r}_1 - \vec{r}_j) \delta(\vec{r}_2 - \vec{r}_k) \right\rangle. \quad (2.4)$$

The pair-correlation function $g(\vec{r}_1, \vec{r}_2)$ is related to $\rho^{(2)}(\vec{r}_1, \vec{r}_2)$ by the relation

$$g(\vec{r}_1, \vec{r}_2) = \frac{\rho^{(2)}(\vec{r}_1, \vec{r}_2)}{\rho(\vec{r}_1)\rho(\vec{r}_2)}. \quad (2.5)$$

The DPCF $c(\vec{r}_1, \vec{r}_2)$, which appears in the expression of free-energy functional $A[\rho]$, is related to the total pair-correlation function $h(\vec{r}_1, \vec{r}_2) = g(\vec{r}_1, \vec{r}_2) - 1$ through the OZ equation (see Ref. [15] for details),

$$c(\vec{r}_1, \vec{r}_2) = h(\vec{r}_1, \vec{r}_2) - \int d\vec{r}_3 c(\vec{r}_1, \vec{r}_3) \rho(\vec{r}_3) h(\vec{r}_2, \vec{r}_3). \quad (2.6)$$

The second functional derivative of $A[\rho]$ is expressed in terms of $c(\vec{r}_1, \vec{r}_2)$ as [2]

$$\frac{\delta^2 A[\rho]}{\delta\rho(\vec{r}_1) \delta\rho(\vec{r}_2)} = \frac{\delta(\vec{r}_1 - \vec{r}_2)}{\rho(\vec{r}_1)} - c(\vec{r}_1, \vec{r}_2), \quad (2.7)$$

where δ is the Dirac function. The first term on the right-hand side of this equation corresponds to ideal part $A_{\text{id}}[\rho]$ of the free energy, whereas the second term corresponds to excess part $A_{\text{ex}}[\rho]$ arising due to interparticle interactions.

In a normal fluid all pair-correlation functions defined above are simple function of number density ρ and depend only on magnitude of interparticle separation $|\vec{r}_2 - \vec{r}_1| = r$. This simplification is due to homogeneity, which implies continuous translational symmetry and isotropy which implies continuous rotational symmetry. In a crystal which is both inhomogeneous and anisotropic, pair-correlation functions can be written as a sum of two terms: one that preserves the continuous symmetry of the fluid and one that breaks it [13,16]. Thus,

$$h(\vec{r}_1, \vec{r}_2) = h^{(0)}(|\vec{r}_2 - \vec{r}_1|, \rho_0) + h^{(b)}(\vec{r}_1, \vec{r}_2; [\rho]), \quad (2.8)$$

$$c(\vec{r}_1, \vec{r}_2) = c^{(0)}(|\vec{r}_2 - \vec{r}_1|, \rho_0) + c^{(b)}(\vec{r}_1, \vec{r}_2; [\rho]). \quad (2.9)$$

While the symmetry-conserving part ($h^{(0)}$ and $c^{(0)}$) depends on the magnitude of interparticle separation r and is a function of average density ρ_0 , the symmetry-broken parts $h^{(b)}$ and $c^{(b)}$ are functional of $\rho(\vec{r})$ (indicated by square bracket) and are invariant only under a discrete set of translations corresponding

to lattice vectors \vec{R}_i ,

$$h^{(b)}(\vec{r}_1, \vec{r}_2) = h^{(b)}(\vec{r}_1 + \vec{R}_i, \vec{r}_2 + \vec{R}_i), \quad (2.10)$$

$$c^{(b)}(\vec{r}_1, \vec{r}_2) = c^{(b)}(\vec{r}_1 + \vec{R}_i, \vec{r}_2 + \vec{R}_i). \quad (2.11)$$

If one chooses a center-of-mass variable $\vec{r}_c = (\vec{r}_1 + \vec{r}_2)/2$ and a difference variable $\vec{r} = \vec{r}_2 - \vec{r}_1$, then one can see from Eqs. (2.10) and (2.11) that $h^{(b)}$ and $c^{(b)}$ are periodic functions of the center-of-mass variable and a continuous function of the difference variable \vec{r} [18]. Thus,

$$h^{(b)}(\vec{r}_1, \vec{r}_2) = \sum_G e^{i\vec{G}\cdot\vec{r}_c} h^{(G)}(\vec{r}), \quad (2.12)$$

$$c^{(b)}(\vec{r}_1, \vec{r}_2) = \sum_G e^{i\vec{G}\cdot\vec{r}_c} c^{(G)}(\vec{r}), \quad (2.13)$$

Since $h^{(G)}$ and $c^{(G)}$ are real and symmetric with respect to interchange of \vec{r}_1 and \vec{r}_2 ; $h^{(-G)}(\vec{r}) = h^{(G)}(\vec{r})$ and $h^{(G)}(-\vec{r}) = h^{(G)}(\vec{r})$ and similar relations hold for $c^{(G)}(\vec{r})$.

Substitution of values of $h(\vec{r}_1, \vec{r}_2)$ and $c(\vec{r}_1, \vec{r}_2)$ given by Eqs. (2.8) and (2.9) in Eq. (2.6) allows us to split the OZ equation into two equations; one that contains $h^{(0)}$, $c^{(0)}$, and ρ_0 while the other contains $h^{(b)}$, $c^{(b)}$, and $\rho(\vec{r}_3)$ along with $h^{(0)}$, $c^{(0)}$, and ρ_0 :

$$\begin{aligned} & h^{(0)}(|\vec{r}_2 - \vec{r}_1|) \\ &= c^{(0)}(|\vec{r}_2 - \vec{r}_1|) + \rho_0 \int d\vec{r}_3 c^{(0)}(|\vec{r}_3 - \vec{r}_1|) h^{(0)}(|\vec{r}_3 - \vec{r}_2|) \end{aligned} \quad (2.14)$$

and

$$\begin{aligned} & h^{(b)}(\vec{r}_1, \vec{r}_2) = c^{(b)}(\vec{r}_1, \vec{r}_2) \\ &+ \int d\vec{r}_3 c^{(0)}(|\vec{r}_3 - \vec{r}_1|) (\rho(\vec{r}_3) - \rho_0) h^{(0)}(|\vec{r}_3 - \vec{r}_2|) \\ &+ \int d\vec{r}_3 \rho(\vec{r}_3) [c^{(b)}(\vec{r}_1, \vec{r}_3) h^{(0)}(|\vec{r}_3 - \vec{r}_2|) \\ &+ c^{(0)}(|\vec{r}_3 - \vec{r}_2|) h^{(b)}(\vec{r}_1, \vec{r}_3) + c^{(b)}(\vec{r}_1, \vec{r}_3) h^{(b)}(\vec{r}_2, \vec{r}_3)]. \end{aligned} \quad (2.15)$$

Equation (2.14) is the well-known OZ equation of normal fluids. We use it along with a closure relation to calculate the values of these correlation functions and their derivatives with respect to density ρ_0 . The derivatives of $c^{(0)}(r)$ are used to find values of three- and four-body direct correlation functions of the isotropic phase.

Equation (2.15) is the OZ equation for the symmetry-broken part of correlation functions. In order to make use of it to find values of $h^{(b)}$ and $c^{(b)}$ for a given $\rho(\vec{r})$ we need one more relation (closure relation) that connects $h^{(b)}$ with $c^{(b)}$. Alternatively, if we know values of one of these functions, then Eq. (2.15) can be used to find values of the other function [19]. Here we calculate $c^{(b)}(\vec{r}_1, \vec{r}_2)$ using a series in ascending powers of $[\rho(\vec{r}) - \rho_0]$.

A. Calculation of $h^{(0)}$, $c^{(0)}$ and their derivatives with respect to ρ

We use the OZ equation (2.14) and a closure relation proposed by Roger and Young (RYC) [20] to calculate pair-correlation functions $h^{(0)}$ and $c^{(0)}$ and their derivatives with respect to ρ in fluids as well as in crystals. The RYC relation joins smoothly the Percus-Yevick (PY) relation and

the hypernetted chain (HNC) relation with an *ad hoc* switching function of intermolecular separation in such a way that at $r = 0$ it reduces to the PY relation and for $r \rightarrow \infty$ it reduces to the HNC relation. The closure relation is written as

$$h^{(0)}(r) = \exp[-\beta u(r)] \left[1 + \frac{\exp[\chi(r)f(r)]}{f(r)} \right] - 1, \quad (2.16)$$

where $\chi(r) = h^{(0)}(r) - c^{(0)}(r)$ and $f(r) = 1 - \exp(-\psi r)$ is the switching function which involves an adjustable parameter $0 \leq \psi \leq \infty$. The value of ψ is chosen to guarantee thermodynamic consistency between the virial and compressibility routes to the equation of state [20]. Though there is no fundamental basis for the RYC, it is able to fix the deficiencies of the PY and the HNC relations in some systems and gives results which are in excellent agreement with simulation results in fluid phase up to the freezing point. For the repulsive potentials (described below) considered in this paper the parameter ψ is density independent. This and the fact that the symmetry-conserving part of pair-correlation functions pass smoothly through the freezing or melting point without getting affected by the symmetry breaking and the OZ relation connecting these functions remains unchanged we extend the method to calculate $h^{(0)}$, $c^{(0)}$ and their derivatives with respect to ρ at densities which correspond to average densities of crystals.

The differentiation of Eqs. (2.14) and (2.16) with respect to ρ yields the following relations:

$$\begin{aligned} \frac{\partial h^{(0)}(r)}{\partial \rho} &= \frac{\partial c^{(0)}(r)}{\partial \rho} + \int d\vec{r}' c^{(0)}(r') h^{(0)}(|\vec{r}' - \vec{r}|) \\ &+ \rho \int d\vec{r}' \frac{\partial c^{(0)}(r')}{\partial \rho} h^{(0)}(|\vec{r}' - \vec{r}|) \\ &+ \rho \int d\vec{r}' c^{(0)}(r') \frac{\partial h^{(0)}(|\vec{r}' - \vec{r}|)}{\partial \rho} \end{aligned} \quad (2.17)$$

and

$$\frac{\partial h^{(0)}(r)}{\partial \rho} = \exp[-\beta u(r)] \exp[\chi(r)f(r)] \frac{\partial \chi(r)}{\partial \rho}, \quad (2.18)$$

$$\begin{aligned} \frac{\partial^2 h^{(0)}(r)}{\partial \rho^2} &= \frac{\partial^2 c^{(0)}(r)}{\partial \rho^2} + 2 \int d\vec{r}' \left[\frac{\partial c^{(0)}(r')}{\partial \rho} h^{(0)}(|\vec{r}' - \vec{r}|) \right. \\ &+ c^{(0)}(r') \frac{\partial h^{(0)}(|\vec{r}' - \vec{r}|)}{\partial \rho} \left. \right] \\ &+ \rho \int d\vec{r}' \left[2 \frac{\partial c^{(0)}(r')}{\partial \rho} \frac{\partial h^{(0)}(|\vec{r}' - \vec{r}|)}{\partial \rho} \right. \\ &+ c^{(0)}(r') \frac{\partial^2 h^{(0)}(|\vec{r}' - \vec{r}|)}{\partial \rho^2} \\ &+ \left. \frac{\partial^2 c^{(0)}(r')}{\partial \rho^2} h^{(0)}(|\vec{r}' - \vec{r}|) \right], \end{aligned} \quad (2.19)$$

and

$$\begin{aligned} \frac{\partial^2 h^{(0)}(r)}{\partial \rho^2} &= \exp[-\beta u(r)] \exp[\chi(r)f(r)] \\ &\times \left[\frac{\partial^2 \chi(r)}{\partial \rho^2} + \left(\frac{\partial \chi(r)}{\partial \rho} \right)^2 f(r) \right]. \end{aligned} \quad (2.20)$$

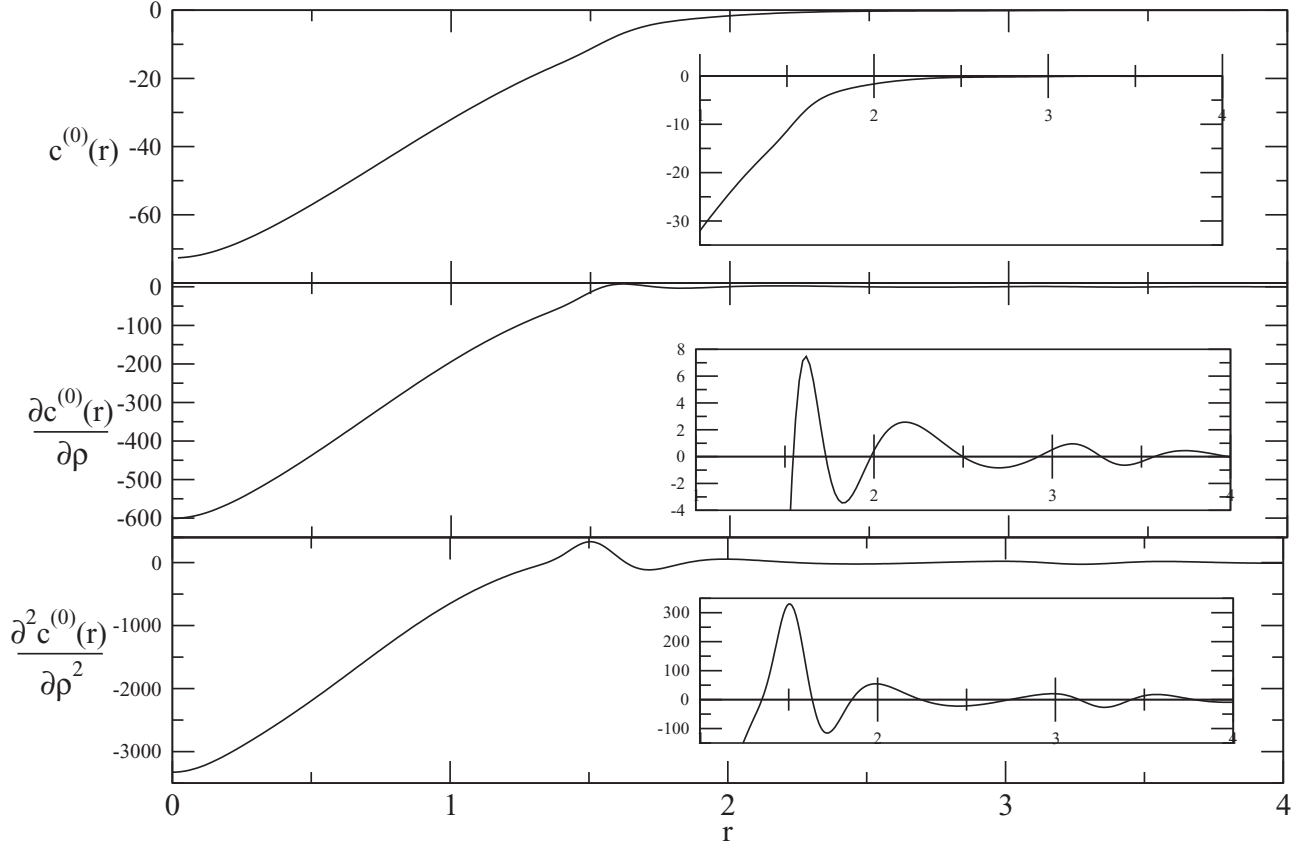


FIG. 1. Plots of $c^{(0)}(r)$, $\frac{\partial c^{(0)}(r)}{\partial \rho}$, and $\frac{\partial^2 c^{(0)}(r)}{\partial \rho^2}$ vs r for $n = 6$ and $\gamma = 2.30$ which is close to the freezing point. The distance r is in unit of $a_0 = (\frac{3}{4\pi\rho})^{1/3}$. Insets show magnified values of respective quantities for $r \geq 1$.

The solution of the closed set of coupled equations (2.14) and (2.17)–(2.20) gives values of $h^{(0)}(r)$, $c^{(0)}(r)$, $\frac{\partial h^{(0)}(r)}{\partial \rho}$, $\frac{\partial c^{(0)}(r)}{\partial \rho}$, $\frac{\partial^2 h^{(0)}(r)}{\partial \rho^2}$, and $\frac{\partial^2 c^{(0)}(r)}{\partial \rho^2}$ as a function of r for a given potential $u(r)$.

The pair potential taken here are the inverse power potentials, $u(r) = \epsilon(\sigma/r)^n$, where ϵ , σ , and n are potential parameters and r is the molecular separation. The parameter n measures softness of the potential, $n = \infty$ corresponds to hard sphere, and $n = 1$ to the one-component plasma. The reason for our choosing these potentials is that the range of potential can be varied by changing the value of n and the fact that the equation of state and melting curves of these potentials have been extensively investigated by computer simulations [21–28] for several values of n so “exact” results are available for comparison. The more repulsive ($n \geq 7$) systems have been found to freeze into a face-centred cubic (fcc) structure while the soft repulsions $n < 7$ freeze into a body-centered cubic crystal (bcc) structure. The fluid-bcc-fcc triple point is found to occur at $\frac{1}{n} \simeq 0.15$ [25,26,28]. The atomic arrangements in the two cubic structures differ substantially; the fcc is close packed in real space and the density inhomogeneity is much sharper than for the bcc, which is open structure in real space but close packed in Fourier space. However, in spite of this difference in the atomic arrangements, the two structures have a small difference in free energy (or chemical potential) at the fluid-solid transition [25–28] and, therefore, a correct description of the relative

stability of the two cubic structures is a stringent test for any theory.

The inverse power potentials are known to have a simple scaling property according to which the reduced thermodynamic properties depend on a single variable which is defined as

$$\gamma = \rho\sigma^3(\beta\epsilon)^{3/n} = \rho^*T^{*(-3/n)},$$

where $\beta = 1/k_B T$, where k_B is the Boltzmann constant and T is temperature. Using the scaling relation the potential is written as

$$\beta u(r) = \left(\frac{4\pi}{3}\gamma\right)^{n/3} \frac{1}{r^n},$$

where r is measured in the unit of $a_0 = (\frac{3}{4\pi\rho})^{1/3}$.

In Fig. 1 we plot values of $c^{(0)}(r)$, $\frac{\partial c^{(0)}(r)}{\partial \rho}$, and $\frac{\partial^2 c^{(0)}(r)}{\partial \rho^2}$ for $n = 6$ and $\gamma = 2.30$, which is close to the freezing point.

B. Calculation of three- and four-body direct correlation functions

The higher-body direct correlation functions can be written as functional derivatives of the DPCF with respect to $\rho(\vec{r})$,

$$c_n(\vec{r}_1, \vec{r}_2, \dots, \vec{r}_n) = \frac{\delta^{n-2} c(\vec{r}_1, \vec{r}_2)}{\delta \rho(\vec{r}_3) \delta \rho(\vec{r}_4) \dots \delta \rho(\vec{r}_n)}.$$

In the limit of a homogeneous fluid this leads to

$$\frac{\partial c^{(0)}(r, \rho_0)}{\partial \rho} = \int d\vec{r}_3 c_3^{(0)}(\vec{r}_1, \vec{r}_2, \vec{r}_3; \rho_0), \quad (2.21)$$

$$\begin{aligned} \frac{\partial^2 c^{(0)}(r, \rho_0)}{\partial \rho^2} &= \int d\vec{r}_3 \frac{c_3^{(0)}(\vec{r}_1, \vec{r}_2, \vec{r}_3; \rho_0)}{\partial \rho} \\ &= \int d\vec{r}_3 \int d\vec{r}_4 c_4^{(0)}(\vec{r}_1, \vec{r}_2, \vec{r}_3, \vec{r}_4; \rho_0), \end{aligned} \quad (2.22)$$

and so on, where $c_m^{(0)}$ is the m -body direct correlation function of the isotropic phase of density ρ_0 . Note that these equations are exact and connect the derivatives of $c^{(0)}(r)$ with respect to density ρ with the higher-body direct correlation functions. Since the values of the derivatives are known as a function of r at a given density, these equations can be solved to find values of $c_3^{(0)}$ and $c_4^{(0)}$. Barrat *et al.* [6] have solved Eq. (2.21) by first writing $c_3^{(0)}$ as a product of an arbitrary function $t(r)$,

$$c_3^{(0)}(\vec{r}_1, \vec{r}_2, \vec{r}_3) = t(r_{12})t(r_{13})t(r_{23}), \quad (2.23a)$$

which allowed separation of variables r_{12} , r_{13} , and r_{23} and then determining the values of $t(r)$ from Eq. (2.21). They compared their results with “exact” molecular-dynamics results near freezing and showed that the factorization ansatz leads to accurate values of $c_3^{(0)}$. We follow their method to calculate values of $c_3^{(0)}$ and extend it to calculate values of $c_4^{(0)}$.

We rewrite Eq. (2.23a) using a diagram as

$$c_3^{(0)}(\vec{r}_1, \vec{r}_2, \vec{r}_3) \equiv \begin{array}{c} \circ^3 \\ \diagup \quad \diagdown \\ \circ^1 \quad \circ^2 \end{array} \quad (2.23b)$$

where a line linking particles i and j denotes a $t(r)$ function and each circle (representing a particle) carry weight unity. Similarly the relation (2.21) is written as

$$\frac{\partial c^{(0)}(r, \rho_0)}{\partial \rho} = \begin{array}{c} \circ^3 \\ \diagup \quad \diagdown \\ \circ^1 \quad \circ^2 \end{array} \quad (2.24)$$

where the half-black circle represents the particle over which integration is performed over its all configurations and all circles carry weight unity. Using known values of $\partial c^{(0)}(r, \rho_0)/\partial \rho_0$ we solve this equation to find values of $t(r)$ for different density ρ_0 (or γ) following a method outlined in Ref. [6]. The values of $t(r)$ as a function of r are shown in Fig. 2 for $n = 6, 4$ and $\gamma = 2.30, 5.60$, respectively.

Taking derivative of both sides of Eq. (2.23a) with respect to ρ_0 one gets

$$\begin{aligned} \frac{\partial c_3^{(0)}(\vec{r}_1, \vec{r}_2, \vec{r}_3)}{\partial \rho_0} &= \frac{\partial t(r_{12})}{\partial \rho_0} t(r_{13}) t(r_{23}) + t(r_{12}) \frac{\partial t(r_{13})}{\partial \rho_0} t(r_{23}) \\ &\quad + t(r_{12}) t(r_{13}) \frac{\partial t(r_{23})}{\partial \rho_0}. \end{aligned} \quad (2.25)$$

Substitution of this into Eq. (2.22) leads to

$$\begin{aligned} \frac{\partial^2 c^{(0)}(r)}{\partial \rho_0^2} &= \int d\vec{r}' \left[\frac{\partial t(r)}{\partial \rho_0} t(r') t(|\vec{r}' - \vec{r}|) + t(r) \frac{\partial t(r')}{\partial \rho_0} t(|\vec{r}' - \vec{r}|) \right. \\ &\quad \left. - \vec{r}|) + t(r) t(r') \frac{\partial t(|\vec{r}' - \vec{r}|)}{\partial \rho_0} \right], \end{aligned} \quad (2.26)$$

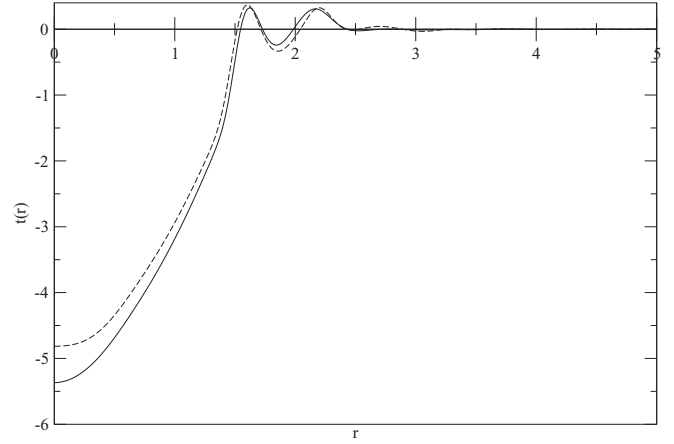


FIG. 2. Plot of $t(r)$ vs r for $n = 6$ at $\gamma = 2.32$ and $n = 4$ at $\gamma = 5.60$. The distance r is in unit of $a_0 = (\frac{3}{4\pi\rho})^{1/3}$. The dashed curve represents values for $n = 4$, $\gamma_1 = 5.60$ and full curve for $n = 6$, $\gamma_1 = 2.32$.

where $r_{12} = r$, $r_{13} = r'$, and $r_{23} = |\vec{r}' - \vec{r}|$. As values of $t(r)$ are known, Eq. (2.26) is used to find values of $\partial t(r)/\partial \rho_0$ in same way as Eq. (2.24) was used to find values of $t(r)$. In Fig. 3 we plot $\partial t(r)/\partial \rho_0$ for $n = 4, 6$ and $\gamma = 5.60, 2.30$.

Guided by the relation of Eq. (2.24) we write $\partial t(r)/\partial \rho_0$ as

$$\begin{aligned} \frac{\partial t(r)}{\partial \rho} &= s(r) \int d\vec{r}'' s(r'') s(|\vec{r}'' - \vec{r}|), \\ &\equiv \begin{array}{c} \circ^3 \\ \diagup \quad \diagdown \\ \circ^1 \quad \circ^2 \end{array} \end{aligned} \quad (2.27)$$

where a dashed line connecting particles i and j is $s(r)$ function. Using the already-determined values of $\partial t(r)/\partial \rho_0$ at a given value of ρ_0 (or γ) we determine values of $s(r)$ in the same way that values of $t(r)$ were determined from known values of $\partial c^{(0)}(r)/\partial \rho_0$. In Fig. 4 we plot values of $s(r)$ for $n = 6, 4$ and $\gamma = 2.30, 5.60$ as a function of r .

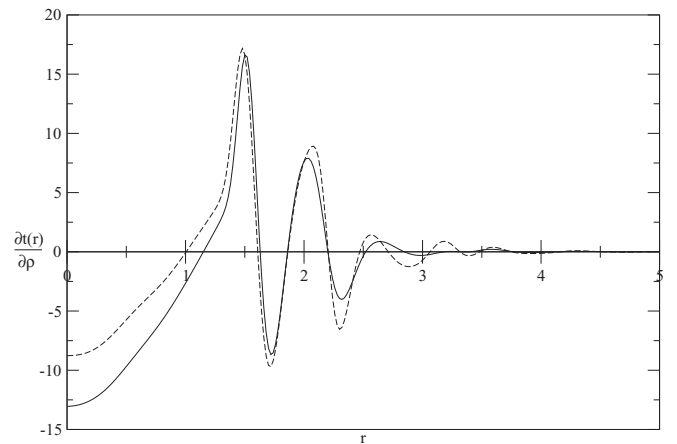


FIG. 3. Plot of $\frac{\partial t(r)}{\partial \rho}$ vs r for $n = 6$ at $\gamma = 2.32$ and $n = 4$ at $\gamma = 5.60$. Other notations are same as in Fig. 2.

From Eqs. (2.22), (2.25), and (2.27) we get

$$c_4^{(0)}(\vec{r}_1, \vec{r}_2, \vec{r}_3, \vec{r}_4) = \begin{array}{c} \text{Diagram 1} \\ + \\ \text{Diagram 2} \\ + \\ \text{Diagram 3} \end{array}, \quad (2.28)$$

where a dashed line represents the $s(r)$ bond and a full line the $t(r)$ bond. We calculate the values of $c_3^{(0)}$ and $c_4^{(0)}$ and plot them in the Appendix.

C. Evaluation of $c^{(b)}(\vec{r}_1, \vec{r}_2)$

The function $c^{(b)}(\vec{r}_1, \vec{r}_2)$ can be expanded in ascending powers of $[\rho(\vec{r}) - \rho_0]$ as [2,13]

$$c^{(b)}(\vec{r}_1, \vec{r}_2; [\rho]) = \int d\vec{r}_3 c_3^{(0)}(\vec{r}_1, \vec{r}_2, \vec{r}_3; \rho_0) [\rho(\vec{r}_3) - \rho_0] + \frac{1}{2} \int d\vec{r}_3 \int d\vec{r}_4 c_4^{(0)}(\vec{r}_1, \vec{r}_2, \vec{r}_3, \vec{r}_4; \rho_0) [\rho(\vec{r}_3) - \rho_0] [\rho(\vec{r}_4) - \rho_0] + \dots, \quad (2.29a)$$

$$\equiv \begin{array}{c} \text{Diagram 1} \\ + \frac{1}{2} \text{Diagram 2} \\ + \frac{1}{2} \text{Diagram 3} \\ + \frac{1}{2} \text{Diagram 4} \\ + \dots \end{array}, \quad (2.29b)$$

where black circles represent integration over all configurations of these particles and each carries weight $\rho(\vec{r}_i) - \rho_0 = \sum_G \rho_G e^{i\vec{G}\cdot\vec{r}_i}$, whereas each white circle carries weight unity. In writing Eq. (2.29b) use has been made of Eqs. (2.23a) and (2.28).

The usefulness of the series of Eq. (2.29) depends on how fast it converges and on our ability to find values of $c_m^{(0)}$. We have already described the calculation of $c_3^{(0)}$ and $c_4^{(0)}$. The same procedure can be used to find $c_m^{(0)}$ for $m > 4$. We, however, find that for a wide range of potentials it is enough to consider the first two terms of the series (2.29). In fact, for most potentials representing the interparticle interactions in real systems one may need to consider the first term only as the contribution

made by the second term to the grand thermodynamic potential at the freezing point turns out to be negligibly small unless the potential has a long-range tail.

1. Evaluation of first term of Eq. (2.29)

Substituting the value of $[\rho(\vec{r}_3) - \rho_0]$ from Eq. (2.3) and using the notations $\vec{r} = \vec{r}_2 - \vec{r}_1$, $\vec{r}' = \vec{r}_3 - \vec{r}_1$, $\vec{r}_c = \frac{1}{2}(\vec{r}_1 + \vec{r}_2)$, we find

$$\begin{array}{c} \text{Diagram 1} \\ \equiv c^{(b,1)}(\vec{r}_1, \vec{r}_2) = \sum_G \rho_G e^{i\vec{G}\cdot\vec{r}_c} t(r) e^{-\frac{1}{2}i\vec{G}\cdot\vec{r}} \\ \times \int d\vec{r}' t(r') t(|\vec{r}' - \vec{r}|) e^{i\vec{G}\cdot\vec{r}'} \end{array} \quad (2.30)$$

This is solved to give [13,14]

$$c^{(b,1)}(\vec{r}_1, \vec{r}_2) = \sum_G e^{i\vec{G}\cdot\vec{r}_c} \sum_{lm} c_l^{(G,1)}(r) Y_{lm}(\hat{r}) Y_{lm}^*(\hat{G}), \quad (2.31)$$

where

$$c_l^{(G,1)}(r) = \rho_G \sum_{l_1} \sum_{l_2} \Lambda_1(l_1, l_2, l) j_{l_2} \left(\frac{1}{2} Gr \right) B_{l_1}(r, G). \quad (2.32)$$

Here $j_l(x)$ is the spherical Bessel function and $Y_{lm}(\hat{x})$ is the spherical harmonics,

$$\begin{aligned} \Lambda_1(l_1, l_2, l) = & (i)^{l_1+l_2} (-1)^{l_2} \left[\frac{(2l_1+1)(2l_2+1)}{(2l+1)} \right]^{\frac{1}{2}} \\ & \times [C_g(l_1, l_2, l; 0, 0, 0)]^2 \end{aligned} \quad (2.33)$$

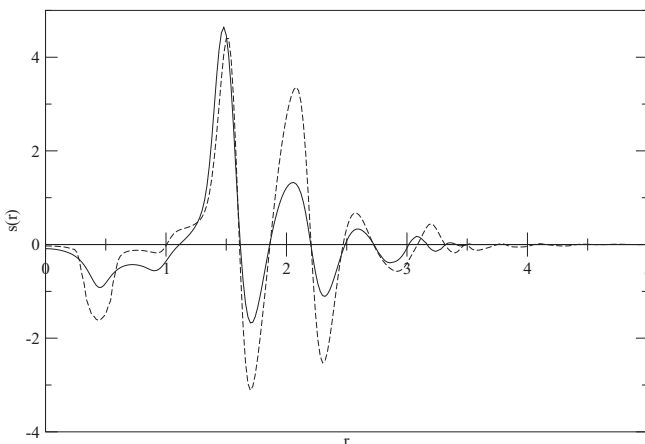


FIG. 4. Plot of $s(r)$ vs r for $n = 6$ at $\gamma = 2.32$ and $n = 4$ at $\gamma = 5.60$. Other notations are same as in Fig. 2.

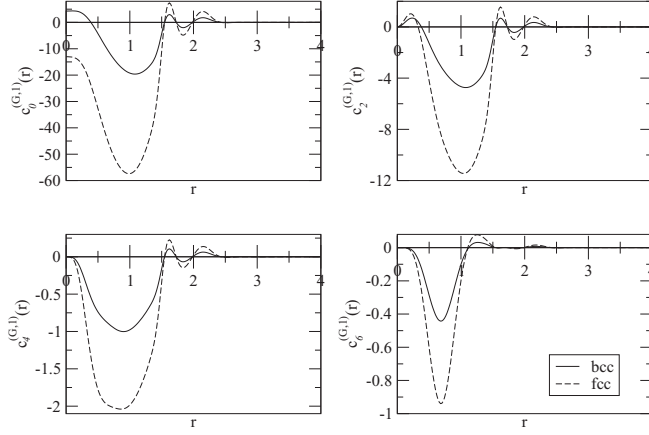


FIG. 5. Comparison of values of $c_l^{(G,1)}(r)$ as a function of r for a G vector of first set of fcc and bcc lattices for $n = 6$, $\gamma_s = 2.32$, $\alpha_{\text{fcc}} = 32$, and $\alpha_{\text{bcc}} = 18$. The distance r is in unit of $a_0 = (\frac{3}{4\pi\rho})^{1/3}$ and $\mu_G = e^{-G^2/4\alpha}$. The dashed curve represents values of fcc structure while full curve of bcc structure.

and

$$B_{l_1}(r, G) = 8t(r) \int dk k^2 t(k) j_{l_1}(kr) \times \int dr' r'^2 t(r') j_{l_1}(kr') j_{l_1}(Gr'), \quad (2.34)$$

where C_g is the Clebsch-Gordan coefficient. The crystal symmetry dictates that l and $l_1 + l_2$ are even and for a cubic crystal, $m = 0, \pm 4$.

The values of $c_l^{(G,1)}(r)$ depend on order parameters $\rho_G = \rho_0 \mu_G$, where $\mu_G = e^{-G^2/4\alpha}$ and α is a localization parameter [see Eq. (3.13)] and on magnitude of \vec{G} . In Figs. 5 and 6 we plot and compare values of $c_l^{(G,1)}(r)$ for bcc and fcc crystals at the melting point for potential $n = 6$, $\gamma_s = 2.32$, $\alpha_{\text{bcc}} = 18$, and $\alpha_{\text{fcc}} = 32$ (see Table I). The values given in these figures are for the first and second sets of RLVs. As expected, the values are far from negligible and differ considerably for the two structures. The value is found to decrease rapidly as the value

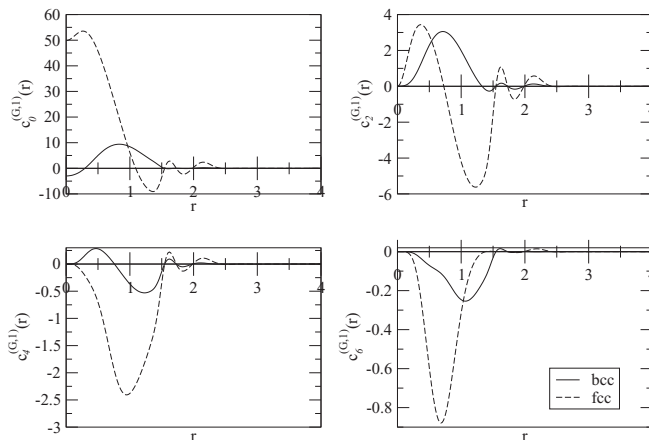


FIG. 6. Comparison of values of $c_l^{(G,1)}(r)$ as a function of r for a G vector of second set of fcc (dashed curve) and bcc (full curve) lattices for $n = 6$, $\gamma_s = 2.32$, $\alpha_{\text{fcc}} = 32$, and $\alpha_{\text{bcc}} = 18$. Other notations are same as in Fig. 5.

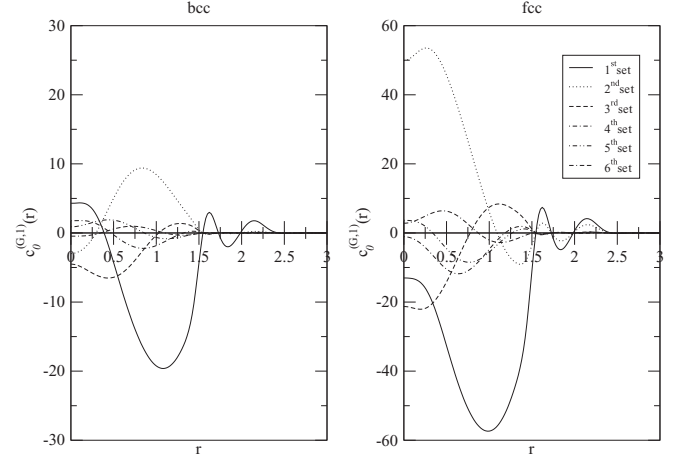


FIG. 7. Comparison of values of $c_0^{(G,1)}(r)$ as a function of r for a G vector of the first six sets of fcc and bcc lattices. The distance r is in unit of $a_0 = (\frac{3}{4\pi\rho})^{1/3}$.

of l is increased; the maximum contribution comes from $l = 0$. We also find, as shown in Fig. 7, the value of $c_l^{(G,1)}(r)$ decreases rapidly as the magnitude of \vec{G} vector increases; the maximum contribution comes from the first two sets of RLVs. The other point to be noted is that, at a given point r , values of $c_l^{(G,1)}(r)$ are positive for some \vec{G} vectors while for others the values are negative, leading to mutual cancellation in a quantity where summation over \vec{G} is involved.

2. Evaluation of second term of Eq. (2.29)

The contribution arising from the second term of Eq. (2.29) is the sum of three diagrams in which the last two contributions are equal. Thus,

$$c^{(b,2)}(\vec{r}_1, \vec{r}_2) = \frac{1}{2} \left[\text{Diagram 1} + \text{Diagram 2} \right]. \quad (2.35)$$

If we write $\vec{r}'' = \vec{r}_4 - \vec{r}_1$ and $\vec{r}_4 = \vec{r}'' + \vec{r}_c - \frac{1}{2}\vec{r}$ and use other notations defined above, the first diagram can be written as

$$\begin{aligned} \frac{1}{2} \left[\text{Diagram 1} \right] &\equiv c^{(b,2,1)}(\vec{r}_1, \vec{r}_2) \\ &= \frac{1}{2} s(r) \sum_{G_1} \sum_{G_2} \rho_{G_1} \rho_{G_2} e^{i(\vec{G}_1 + \vec{G}_2) \cdot (\vec{r}_c - \frac{1}{2}\vec{r})} \\ &\quad \times \int d\vec{r}' t(r') t(|\vec{r}' - \vec{r}|) e^{i\vec{G}_1 \cdot \vec{r}'} \\ &\quad \times \int d\vec{r}'' s(r'') s(|\vec{r}'' - \vec{r}|) e^{i\vec{G}_2 \cdot \vec{r}''}. \quad (2.36) \end{aligned}$$

This is solved to give

$$c^{(b,2,1)}(\vec{r}_1, \vec{r}_2) = \sum_G e^{i\vec{G} \cdot \vec{r}_c} \sum_{lm} \sum_{l'm'} c_{lm, l'm'}^{(G,2,1)}(r) Y_{l'm'}^*(\hat{G}) Y_{lm}(\hat{r}), \quad (2.37)$$

TABLE I. Freezing parameters γ_l , $\Delta\gamma$ and the contributions of ideal symmetry-conserving and symmetry-broken parts arising from first and second terms of Eq. (2.29) to $\Delta W/N$ at the transition point.

n	Lattice	γ_l	$\Delta\gamma$	$\Delta W_{id}/N$	$\Delta W_o/N$	$\Delta W_b^{(1)}/N$	$\Delta W_b^{(2)}/N$
4	bcc	5.57	0.007	2.86	-2.09	-0.94	0.17
	fcc	5.60	0.008	3.52	-2.64	-1.03	0.15
6	bcc	2.30	0.011	2.56	-1.99	-0.58	0.01
	fcc	2.32	0.012	3.48	-2.75	-0.72	0.002
6.5	bcc	2.04	0.014	2.38	-1.89	-0.50	0.001
	fcc	2.03	0.013	3.34	-2.69	-0.66	0.001
7	bcc	1.86	0.015	2.29	-1.85	-0.44	0.000
	fcc	1.84	0.014	3.39	-2.76	-0.63	0.000
12	fcc	1.17	0.034	3.71	-3.14	-0.57	0.000
∞	fcc	0.937	0.106	4.44	-4.10	-0.34	0.000

where

$$c_{lm,l'm'}^{(G,2,1)}(r) = \sum_{G_1} \rho_{G_1} \rho_K \sum_{l_1 m_1} \sum_{l_2 m_2} \Lambda_{mm'm_1 m_2}^{ll'l_1 l_2} M_{l_1}(r, G_1) M_{l_2}(r, K) \times j_{l'} \left(\frac{1}{2} Gr \right) Y_{l_1 m_1}^*(\hat{G}_1) Y_{l_2 m_2}^*(\hat{K}). \quad (2.38)$$

Here $\vec{K} = \vec{G} - \vec{G}_1$,

$$\Lambda_{mm'm_1 m_2}^{ll'l_1 l_2} = 16 \sum_{l_3 m_3} (i)^{l_1+l_2+l'} (-1)^{l'} \left[\frac{(2l_1+1)(2l_2+1)(2l'+1)}{(2l+1)} \right]^{1/2} \times C_g(l_1, l_2, l_3; 0, 0, 0) C_g(l', l_3, l; 0, 0, 0) \times C_g(l_1, l_2, l_3; m_1, m_2, m_3) C_g(l', l_3, l; m', m_3, m), \quad (2.39)$$

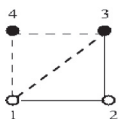
$$M_{l_1}(r, G_1) = \int dr' r'^2 j_{l_1}(Gr') t(r') \int dk k^2 t(k) j_{l_1}(kr) j_{l_1}(kr'), \quad (2.40)$$

and

$$M_{l_2}(r, K) = \int dr'' r''^2 j_{l_2}(Kr'') s(r'') \times \int dk k^2 s(k) j_{l_2}(kr) j_{l_2}(kr''). \quad (2.41)$$

The crystal symmetry dictates that all l_i are even and for a cubic crystal all m_i are 0 and ± 4 .

From the second diagram of Eq. (2.35) we get



$$\equiv c^{(b,2,2)}(\vec{r}_1, \vec{r}_2) = t(r) \sum_{G_1} \sum_{G_2} \rho_{G_1} \rho_{G_2} \times e^{i(\vec{G}_1 + \vec{G}_2) \cdot (\vec{r}_c - \frac{1}{2} \vec{r})} \int d\vec{r}' s(r') t(|\vec{r}' - \vec{r}|) e^{i\vec{G}_1 \cdot \vec{r}'} \times \int d\vec{r}'' s(r'') s(|\vec{r}'' - \vec{r}'|) e^{i\vec{G}_1 \cdot \vec{r}''}. \quad (2.42)$$

This is solved to give

$$c^{(b,2,2)}(\vec{r}_1, \vec{r}_2) = \sum_G e^{i\vec{G} \cdot \vec{r}_c} \sum_{lm} \sum_{l'm'} c_{lm,l'm'}^{(G,2,2)}(r) Y_{l'm'}^*(\hat{G}) Y_{lm}(\hat{r}), \quad (2.43)$$

where

$$c_{lm,l'm'}^{(G,2,2)}(r) = \sum_{G_1} \rho_{G_1} \rho_K \sum_{l_1 m_1} \sum_{l_2 m_2} \sum_{l_3 m_3} \Lambda_{mm'm_1 m_2 m_3}^{ll'l_1 l_2 l_3} N_{l_1, l_2, l_3}(r, G, G_1) \times j_{l'} \left(\frac{1}{2} Gr \right) Y_{l_1 m_1}^*(\hat{G}_1) Y_{l_2 m_2}^*(\hat{K}), \quad (2.44)$$

$$\Lambda_{mm'm_1 m_2 m_3}^{ll'l_1 l_2 l_3} = 32 (i)^{l_1+l_2+l'} (-1)^{l'} \left[\frac{(2l_1+1)(2l_2+1)(2l'+1)}{(2l+1)} \right]^{1/2} \times C_g(l_1, l_2, l_3; 0, 0, 0) C_g(l', l_3, l; 0, 0, 0) \times C_g(l_1, l_2, l_3; m_1, m_2, m_3) C_g(l', l_3, l; m', m_3, m), \quad (2.45)$$

$$N_{l_1, l_2, l_3}(r, G, G_1)$$

$$= t(r) \int dr' r'^2 s(r') j_{l_1}(G_1 r') B_{l_2}(r', K) A_{l_3}(r, r'), \quad (2.46)$$

$$A_{l_3}(r, r') = \int dk k^2 t(k) j_{l_3}(kr) j_{l_3}(kr'), \quad (2.47)$$

and

$$B_{l_2}(r', K) = \int dr'' r''^2 j_{l_2}(Kr'') s(r'') \times \int dk k^2 s(k) j_{l_2}(kr') j_{l_2}(kr''). \quad (2.48)$$

The total contribution arising from the second term of Eq. (2.29) is

$$c^{(b,2)}(\vec{r}_1, \vec{r}_2) = \sum_G e^{i\vec{G} \cdot \vec{r}_c} \sum_{lm} \sum_{l'm'} [c_{lm,l'm'}^{(G,2,1)}(r) + c_{lm,l'm'}^{(G,2,2)}(r)] \times Y_{lm}(\hat{r}) Y_{l'm'}^*(\hat{G}), \quad (2.49)$$

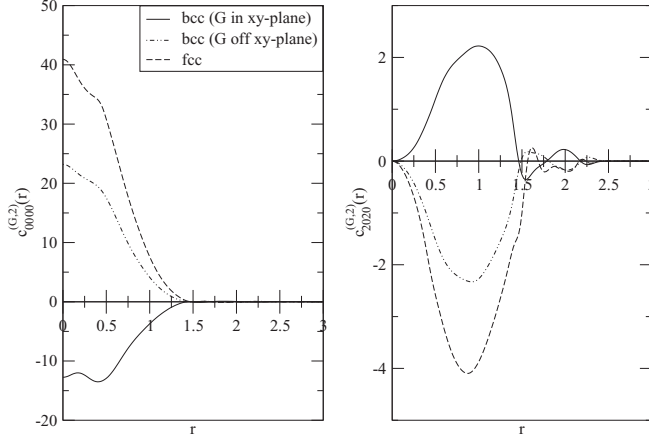


FIG. 8. Comparison of values of $c_{lml'm'}^{(G,2)}(r)$ as a function of r for a G vector of the first set of fcc and bcc lattices for $n = 6$ at $\gamma_s = 2.32$, $\alpha_{\text{fcc}} = 32$, and $\alpha_{\text{bcc}} = 18$. The distance r is in unit of $a_0 = (\frac{3}{4\pi\rho})^{1/3}$. There are two sets of values for the bcc lattice, one for \vec{G} vectors lying in x - y plane and the other for the rest of the \vec{G} vectors of the first set. There is only one set of values for the fcc lattice.

where l, l' are even and $m = 0, \pm 4$ for cubic lattices. In Figs. 8 and 9 we plot values of

$$c_{lml'm'}^{(G,2)}(r) = c_{lml'm'}^{(G,2,1)}(r) + c_{lml'm'}^{(G,2,2)}(r), \quad (2.50)$$

as a function of r for bcc and fcc structures for $n = 6$, $\gamma_s = 2.32$, $\alpha_{\text{bcc}} = 18$, and $\alpha_{\text{fcc}} = 32$. The values given in these figures are for the first two sets of RLVs for $l = l' = 0$ and 2 and $m = m' = 0$. These are the terms which mostly contribute to $c_{lml'm'}^{(G,2)}(r)$; the contributions from terms $l \neq l'$ and $m \neq m'$ are approximately an order of magnitude smaller. For a bcc lattice we find two sets of values, one for \vec{G} vectors lying in the x - y plane and the other for the rest of the vectors. Since all vectors of the first set of RLVs of a fcc lattice are from the x - y plane we get only one set of values. For the second set of RLVs of a fcc lattice, two sets of values are found but they are

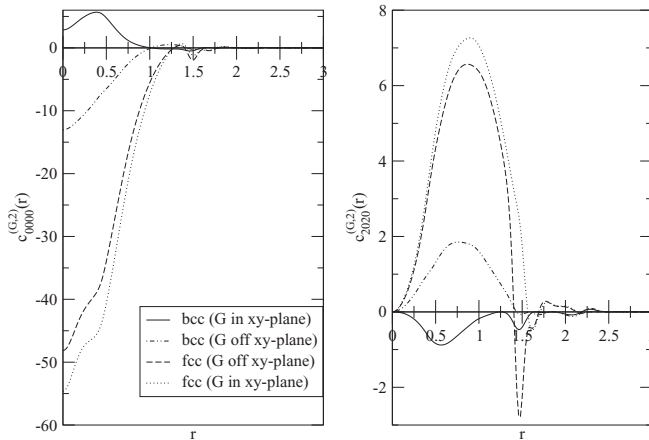


FIG. 9. Comparison of the values of $c_{lml'm'}^{(G,2)}(r)$ as a function of r for a G vector of the second set of fcc and bcc lattices. Other notations are same as in Fig. 8, except that there is now two sets of values shown by dashed and dotted curves for fcc lattice (see text).

close, unlike in the case of the bcc lattice where the two sets of values differ not only in magnitude but also in sign. The values differ considerably for the two cubic structures. The value of $c_{lml'm'}^{(G,2)}(r)$ decreases rapidly for both bcc and fcc structures as the magnitude of \vec{G} vectors increases, as was found in the case of $c_l^{(G,1)}(r)$. Furthermore, the values of $c_{lml'm'}^{(G,2)}(r)$ at a given value of r is positive for some \vec{G} vector and negative for others.

In order to compare the magnitude of contributions made by the first and second terms of Eq. (2.29), we calculate $\hat{c}^{(G,1)}(k, \theta_k, \phi_k)$ and $\hat{c}^{(G,2)}(k, \theta_k, \phi_k)$, defined as

$$\begin{aligned} \hat{c}^{(G,1)}(k, \theta_k, \phi_k) &= \rho \sum_{lm} \int d\vec{r} c_l^{(G,1)}(r) e^{i\vec{k}\cdot\vec{r}} Y_{lm}(\hat{r}) Y_{lm}^*(\hat{G}) \\ &= 4\pi \rho \sum_{lm} (i)^l Y_{lm}(\hat{k}) Y_{lm}^*(\hat{G}) \\ &\quad \times \int_0^\infty dr r^2 c_l^{(G,1)}(r) j_l(kr) \end{aligned} \quad (2.51)$$

and

$$\begin{aligned} \hat{c}^{(G,2)}(k, \theta_k, \phi_k) &= \rho \sum_{lm} \sum_{l'm'} \int d\vec{r} c_{lml'm'}^{(G,2)}(r) e^{i\vec{k}\cdot\vec{r}} Y_{lm}(\hat{r}) Y_{l'm'}^*(\hat{G}) \\ &= 4\pi \rho \sum_{lm} \sum_{l'm'} (i)^l Y_{lm}(\hat{k}) Y_{l'm'}^*(\hat{G}) \\ &\quad \times \int_0^\infty dr r^2 c_{lml'm'}^{(G,2)}(r) j_l(kr). \end{aligned} \quad (2.52)$$

In Figs. 10 and 11 we compare, using color codes (shown on the right-hand side of each figure), the values of these functions arising from the first and second terms of Eq. (2.29) for both fcc and bcc structures for $n = 6$, $\gamma_s = 2.32$, $\alpha_{\text{fcc}} = 32$, and $\alpha_{\text{bcc}} = 18$. The values given in Fig. 10 are for a fcc lattice for a \vec{G} vector of first and a vector of second sets, i.e., $G_1 a_0 = 4.25$, $\theta_{G_1} = 54.7^\circ$, and $\phi_{G_1} = 45^\circ$ and $G_2 a_0 = 4.91$, $\theta_{G_2} = 0^\circ$, $\phi_{G_2} = 90^\circ$. The values of ka_0 are taken to be equal to 4.25 and 4.91 which are the magnitude of $G_1 a_0$ and $G_2 a_0$, respectively. In Fig. 11 we compare the values of $\hat{c}^{(G,1)}(k, \theta_k, \phi_k)$ and $\hat{c}^{(G,2)}(k, \theta_k, \phi_k)$ for a bcc lattice for $G_1 a_0 = 4.37$, $\theta_{G_1} = 90^\circ$, $\phi_{G_1} = 45^\circ$ and $G_2 a_0 = 6.19$, $\theta_{G_2} = 90^\circ$, $\phi_{G_2} = 0^\circ$ and $ka_0 = 4.37$ and 6.19. From these figures it is clear that the contribution made by the second term to $c^{(b)}(\vec{r}_1, \vec{r}_2)$ is small compared to the first term, indicating fast convergence of the series. As is shown below, in the expression of the free-energy functional, $c^{(b)}(\vec{r}_1, \vec{r}_2)$ is averaged over density and order parameters and also there is summation over \vec{G} vectors, As a consequence, the contribution of second term of Eq. (2.29) is found to be an order of magnitude smaller than the first term. We show that the consideration of the first two terms of Eq. (2.29) is enough to give an accurate description of the freezing transitions for a wide class of potentials.

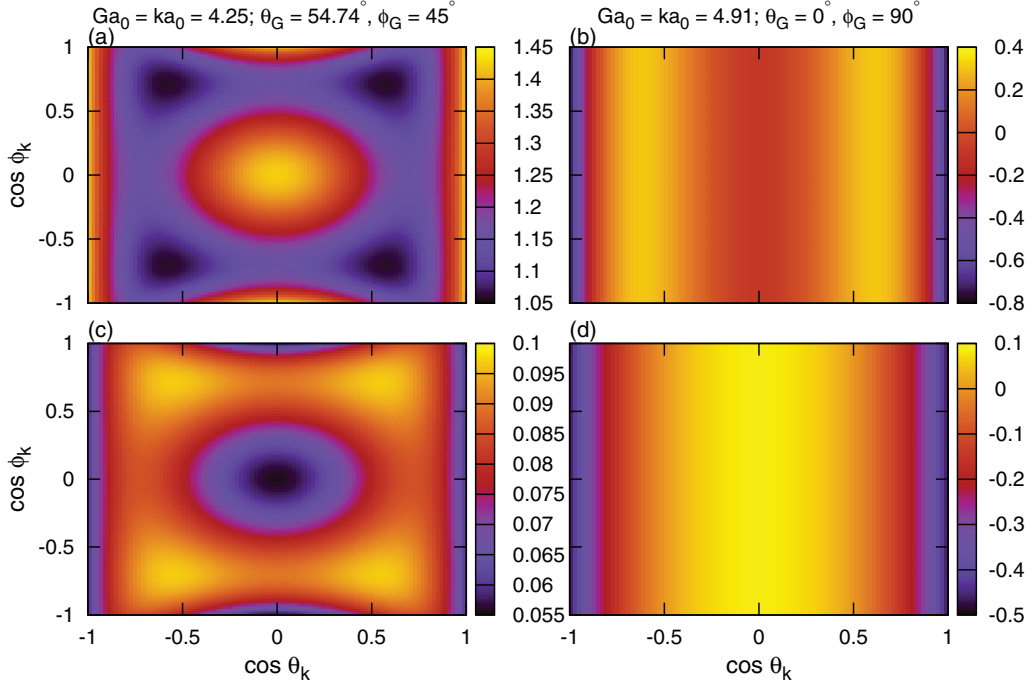


FIG. 10. (Color online) Comparison of values (shown using color codes given on right-hand side of each figure) of $c^{(G,1)}(k, \theta_k, \phi_k)$ [(a) and (b)] and $c^{(G,2)}(k, \theta_k, \phi_k)$ [(c) and (d)] as a function of $\cos \theta_k$ (plotted on x axis) and $\cos \phi_k$ (plotted on y axis) for $G_1 a_0 = ka_0 = 4.25$, $\theta_{G_1} = 54.7^\circ$, $\phi_{G_1} = 45^\circ$ [(a) and (c)] and $G_2 a_0 = ka_0 = 4.91$, $\theta_{G_2} = 0^\circ$, $\phi_{G_2} = 90^\circ$ [(b) and (d)] for a fcc lattice for $n = 6$, $\gamma_s = 2.32$, $\alpha_{fcc} = 32$.

III. FREE-ENERGY FUNCTIONAL AND FLUID-SOLID TRANSITION

The reduced free-energy functional $A[\rho]$ of a symmetry-broken phase can be written as [13,14,17]

$$A[\rho] = A_{id}[\rho] + A_{ex}^{(0)}[\rho] + A_{ex}^{(b)}[\rho], \quad (3.1)$$

where

$$A_{id}[\rho] = \int d\vec{r} \rho(\vec{r}) [\ln(\rho(\vec{r})\Lambda) - 1], \quad (3.2)$$

$$A_{ex}^{(0)}[\rho]$$

$$= A_{ex}(\rho_l) + \beta(\mu - \ln(\rho_l \Lambda)) \int d\vec{r} (\rho(\vec{r}) - \rho_l) - \frac{1}{2} \int d\vec{r}_1 \int d\vec{r}_2 (\rho(\vec{r}_1) - \rho_l)(\rho(\vec{r}_2) - \rho_l) \bar{c}^{(0)}(|\vec{r}_2 - \vec{r}_1|), \quad (3.3)$$

and

$$A_{ex}^{(b)}[\rho] = -\frac{1}{2} \int d\vec{r}_1 \int d\vec{r}_2 (\rho(\vec{r}_1) - \rho_0)(\rho(\vec{r}_2) - \rho_0) \bar{c}^{(b)}(\vec{r}_1, \vec{r}_2). \quad (3.4)$$

Here Λ is the cube of the thermal wavelength associated with a molecule, $\beta = (k_B T)^{-1}$, where k_B is the Boltzmann constant and T is the temperature, $A_{ex}^{(0)}(\rho_l)$ is the excess reduced free energy of the coexisting isotropic fluid of density ρ_l and the chemical potential μ , and $\rho_0 = \rho_l (1 + \Delta\rho^*)$ is the

average density of the solid,

$$\bar{c}^{(0)}(|\vec{r}_2 - \vec{r}_1|) = 2 \int_0^1 d\lambda \lambda \int_0^1 d\lambda' c^{(0)}(|\vec{r}_2 - \vec{r}_1|; \rho_l + \lambda\lambda'(\rho_0 - \rho_l)) \quad (3.5)$$

and

$$\bar{c}^{(b)}(\vec{r}_1, \vec{r}_2) = 4 \int_0^1 d\lambda \lambda \int_0^1 d\lambda' \int_0^1 d\xi \xi \int_0^1 d\xi' \xi' c^{(b)}(\vec{r}_1, \vec{r}_2; \lambda\lambda'\rho_0, \xi\xi'\rho_G). \quad (3.6)$$

As the density difference between the solid and the coexisting fluid at the freezing point is very small, $\bar{c}^{(0)}(|\vec{r}_2 - \vec{r}_1|, \rho_0)$ can, as shown below, be replaced by $c^{(0)}(r, \rho_l)$. This reduces Eq. (3.3) to the one that appears in the RY functional.

The expression for the symmetry-conserving part of the reduced excess free energy $A_{ex}^{(0)}[\rho]$ given by Eq. (3.3) is found by performing double functional integration of [13,17]

$$\frac{\delta^2 A_{ex}^{(0)}[\rho]}{\delta\rho(\vec{r}_1) \delta\rho(\vec{r}_2)} = -c^{(0)}(|\vec{r}_2 - \vec{r}_1|). \quad (3.7)$$

This integration is carried out in the density space, taking the coexisting uniform fluid of density ρ_l and the chemical potential μ as a reference. The expression for the symmetry-broken part $A_{ex}^{(b)}[\rho]$ given by Eq. (3.4) is found by performing double functional integration of [13,17]

$$\frac{\delta^2 A_{ex}^{(b)}[\rho]}{\delta\rho(\vec{r}_1) \delta\rho(\vec{r}_2)} = -c^{(b)}(\vec{r}_1, \vec{r}_2) \quad (3.8)$$

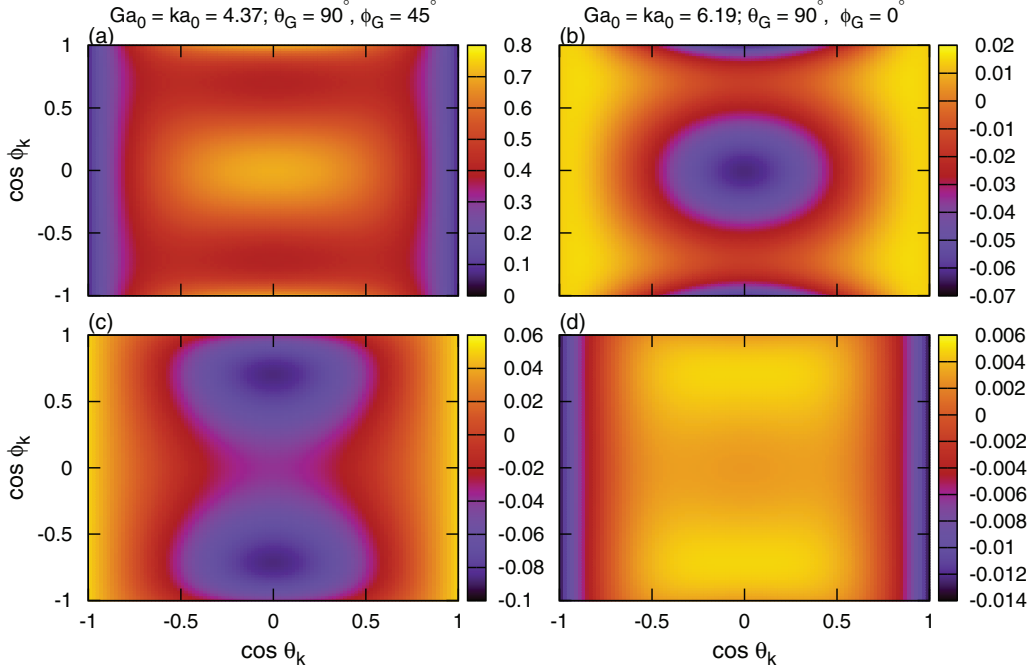


FIG. 11. (Color online) Comparison of values (given in a color code) of $c^{(G,1)}(k, \theta_k, \phi_k)$ [(a) and (b)] and $c^{(G,2)}(k, \theta_k, \phi_k)$ [(c) and (d)] as a function of $\cos \theta_k$ and $\cos \phi_k$ for $G_1 a_0 = ka_0 = 4.37$, $\theta_{G_1} = 90^\circ$, $\phi_{G_1} = 45^\circ$ [(a) and (c)] and $G_2 a_0 = ka_0 = 6.19$, $\theta_{G_2} = 90^\circ$, $\phi_{G_2} = 0^\circ$ [(b) and (d)] for a bcc lattice for $n = 6$, $\gamma_s = 2.32$, $\alpha_{\text{bcc}} = 18$. Other notation are same as in Fig. 10.

in the density space corresponding to the symmetry-broken phase. The path of integration in this space is characterized by two parameters, λ and ξ . These parameters vary from 0 to 1. The parameter λ raises the density from zero to the final value ρ_0 as it varies from 0 to 1, whereas parameter ξ raises the order parameter from 0 to its final value ρ_G . The result is independent of the order of integration.

In locating the transition the grand thermodynamic potential defined as

$$-W = A - \beta\mu \int d\vec{r} \rho(\vec{r}) \quad (3.9)$$

is generally used as it ensures that the pressure and chemical potential of both phases remain equal at the transition. The transition point is determined by the condition $\Delta W = W_l - W = 0$, where W_l is the grand thermodynamic potential of the coexisting fluid. The expression of ΔW is found to be [13,14]

$$\begin{aligned} \Delta W = & \int d\vec{r} \left[\rho(\vec{r}) \ln \left(\frac{\rho(\vec{r})}{\rho_l} \right) - (\rho(\vec{r}) - \rho_l) \right] \\ & - \frac{1}{2} \int d\vec{r}_1 \int d\vec{r}_2 (\rho(\vec{r}_1) - \rho_l)(\rho(\vec{r}_2) - \rho_l) \tilde{c}^{(0)}(|\vec{r}_2 - \vec{r}_1|) \\ & - \frac{1}{2} \int d\vec{r}_1 \int d\vec{r}_2 (\rho(\vec{r}_1) - \rho_0)(\rho(\vec{r}_2) - \rho_0) \tilde{c}^{(b)}(\vec{r}_1, \vec{r}_2). \end{aligned} \quad (3.10)$$

Minimization of ΔW with respect to $\rho(\vec{r})$ subject to the perfect crystal constraint leads to

$$\begin{aligned} \ln \frac{\rho(\vec{r}_1)}{\rho_l} = & \phi + \int d\vec{r}_2 [\rho(\vec{r}_2) - \rho_l] \tilde{c}^{(0)}(|\vec{r}_2 - \vec{r}_1|) \\ & + \int d\vec{r}_2 [\rho(\vec{r}_2) - \rho_0] \tilde{c}^{(b)}(\vec{r}_1, \vec{r}_2), \end{aligned} \quad (3.11)$$

where

$$\tilde{c}^{(0)}(|\vec{r}_2 - \vec{r}_1|) = \int_0^1 d\lambda c^{(0)}[|\vec{r}_2 - \vec{r}_1|; \rho_l + \lambda(\rho_0 - \rho_l)]$$

and

$$\tilde{c}^{(b)}(\vec{r}_1, \vec{r}_2) = \int_0^1 d\lambda \int_0^1 d\xi c^{(b)}(\vec{r}_1, \vec{r}_2; \lambda \rho_0, \xi \rho_G).$$

The value of the Lagrange multiplier ϕ in Eq. (3.11) is found from the condition

$$\frac{1}{V} \int d\vec{r} \frac{\rho(\vec{r})}{\rho_0} = 1, \quad (3.12)$$

where V is volume of the system.

It may be noted that, in principle, one needs only values of symmetry-conserved and symmetry-broken parts of the DPCF to determine $\rho(\vec{r})$ that minimizes the grand potential W . In practice, however, it is found convenient to do minimization with respect to an assumed form of $\rho(\vec{r})$. The ideal part is calculated using a form of $\rho(\vec{r})$ which is a superposition of normalized Gaussians centered around the lattice sites,

$$\rho(\vec{r}) = \left(\frac{\alpha}{\pi} \right)^{3/2} \sum_n \exp[-\alpha(\vec{r} - \vec{R}_i)^2], \quad (3.13)$$

where α is the variational parameter that characterizes the width of the Gaussian and the square root of α is inversely proportional to the width of a peak. It thus measures the nonuniformity; $\alpha = 0$ corresponds to the limit of a uniform fluid and an increasing value of α corresponds to increasing localization of particles on their respective lattice sites defined by vectors \vec{R}_i . For the interaction part it is convenient to use the

expression of $\rho(\vec{r})$ given by Eq. (2.3). The Fourier transform of Eq. (3.13) leads to $\rho_G = \rho_0 \mu_G$, where $\mu_G = e^{-G^2/4\alpha}$.

A. Evaluation of $\bar{c}^{(0)}(r)$ and $\bar{c}^{(b)}(\vec{r}_1, \vec{r}_2)$

The values of $\bar{c}^{(0)}(r)$ for a given fluid density ρ_l and the average crystal density ρ_0 are found from the known values of $c^{(0)}(r, \rho)$, where ρ varies from ρ_l to ρ_0 by performing integrations in Eq. (3.5) which can be rewritten as

$$\bar{c}^{(0)}(r, \rho_0) = 2 \int_0^1 d\lambda \lambda \int_0^1 d\lambda' c^{(0)}(r; \rho_l(1 + \lambda\lambda' \Delta\rho^*)), \quad (3.14)$$

where $\Delta\rho^* = (\rho_0 - \rho_l)/\rho_l$. The integrations have been done numerically using a very fine grid for variables λ and λ' . As the system in the density range of ρ_l to $\rho_l(1 + \Delta\rho^*)$ is inhomogeneous due to nucleation, the density that appears in Eq. (3.14) corresponds to the averaged density. Since at the freezing point $\rho_l \Delta\rho^* \ll 1$, one can use Taylor expansion to solve Eq. (3.14), leading to

$$\bar{c}^{(0)}(r, \rho_0) = c^{(0)}(r, \rho_l) + \frac{1}{3} \rho_l \Delta\rho^* \frac{\partial c^{(0)}(r, \rho_l)}{\partial \rho_l} + O(\rho_l^2 \Delta\rho^{*2}). \quad (3.15)$$

The contribution arising from the second term in the free energy is found to be negligibly small, suggesting the replacement of $\bar{c}^{(0)}(r, \rho_0)$ by $c^{(0)}(r, \rho_l)$.

Since the order parameters that appear in $\bar{c}^{(b)}(\vec{r}_1, \vec{r}_2)$ are linear in $c^{(b,1)}(\vec{r}_1, \vec{r}_2)$ and quadratic in $c^{(b,2)}(\vec{r}_1, \vec{r}_2)$, the integration over ξ variables in Eq. (3.4) can be performed analytically, leading to

$$\begin{aligned} \bar{c}^{(b)}(\vec{r}_1, \vec{r}_2) &= \sum_G e^{i\vec{G} \cdot \vec{r}_c} \left[\sum_{lm} \bar{c}_l^{(G,1)}(r) Y_{lm}^*(\hat{G}) Y_{lm}(\hat{r}) \right. \\ &\quad \left. + \sum_{lm} \sum_{l'm'} (\bar{c}_{lm, l'm'}^{(G,2,1)}(r) + \bar{c}_{lm, l'm'}^{(G,2,2)}(r)) Y_{l'm'}^*(\hat{G}) Y_{lm}(\hat{r}) \right], \end{aligned} \quad (3.16)$$

where

$$\bar{c}_l^{(G,1)}(r) = \frac{1}{3} \rho_G \sum_{l_1} \sum_{l_2} \Lambda_1(l_1, l_2, l) j_{l_2} \left(\frac{1}{2} Gr \right) \bar{B}_{l_1}(r, G), \quad (3.17)$$

$$\begin{aligned} \bar{c}_{lm, l'm'}^{(G,2,1)}(r) &= \frac{1}{6} \sum_{G_1} \rho_{G_1} \rho_K \sum_{l_1 m_1} \sum_{l_2 m_2} \Lambda_{mm'm_1 m_2}^{ll'l_1 l_2} j_{l'} \left(\frac{1}{2} Gr \right) \\ &\quad \times \bar{Q}_{l_1 l_2}(r, G, G_1) Y_{l_1 m_1}^*(\hat{G}_1) Y_{l_2 m_2}^*(\hat{K}), \end{aligned} \quad (3.18)$$

$$\begin{aligned} \bar{c}_{lm, l'm'}^{(G,2,2)}(r) &= \frac{1}{6} \sum_{G_1} \rho_{G_1} \rho_K \sum_{l_1 m_1} \sum_{l_2 m_2} \sum_{l_3 m_3} \Lambda_{mm'm_1 m_2 m_3}^{ll'l_1 l_2 l_3} j_{l'} \left(\frac{1}{2} Gr \right) \\ &\quad \times \bar{N}_{l_1 l_2 l_3}(r, G, G_1) Y_{l_2 m_2}^*(\hat{G}_1) Y_{l_3 m_3}^*(\hat{K}), \end{aligned} \quad (3.19)$$

with

$$\bar{B}_{l_1}(r, G) = 2 \int_0^1 d\lambda \lambda \int_0^1 d\lambda' B_{l_1}(r, G; \lambda\lambda' \rho), \quad (3.20)$$

$$\begin{aligned} \bar{Q}_{l_1 l_2}(r, G, G_1) &= 2 \int_0^1 d\lambda \lambda \int_0^1 d\lambda' Q_{l_1 l_2}(r, G, G_1; \lambda\lambda' \rho), \\ Q_{l_1 l_2}(r, G, G_1; \rho) &= M_{l_1}(r, G_1; \rho) M_{l_2}(r, K; \rho), \end{aligned} \quad (3.21)$$

and

$$\bar{N}_{l_1 l_2 l_3}(r, G, G_1) = 2 \int_0^1 d\lambda \lambda \int_0^1 d\lambda' N_{l_1 l_2 l_3}(r, G, G_1; \lambda\lambda' \rho). \quad (3.22)$$

The quantities $B_{l_1}(r, G)$, $M_{l_1}(r, G_1)$, $M_{l_2}(r, K)$, and $N_{l_1 l_2 l_3}(r, G, G_1)$ are defined by Eqs. (2.34), (2.40), (2.41), and (2.46), respectively. The integrations over λ and λ' have been performed numerically by varying them from 0 to 1 on a fine grid and evaluating the functions B_{l_1} , $Q_{l_1 l_2}$, and $N_{l_1 l_2 l_3}$ on these densities. Since these functions vary smoothly with density and their values have been evaluated at closely spaced values of density, the result found for $\bar{c}^{(b)}(\vec{r}_1, \vec{r}_2)$ is expected to be accurate.

B. Evaluation of ΔW

Substituting expression of $\rho(\vec{r})$ given by Eqs. (2.3) and (3.14) and of $\bar{c}^{(0)}(r)$ and $\bar{c}^{(b)}(\vec{r}_1, \vec{r}_2)$ given above in Eq. (3.10) we find

$$\frac{\Delta W}{N} = \frac{\Delta W_{\text{id}}}{N} + \frac{\Delta W_0}{N} + \frac{\Delta W_b^{(1)}}{N} + \frac{\Delta W_b^{(2)}}{N}, \quad (3.23)$$

where

$$\frac{\Delta W_{\text{id}}}{N} = 1 - (1 + \Delta\gamma) \left[\frac{5}{2} + \ln \rho_l - \frac{3}{2} \ln \left(\frac{\alpha}{\pi} \right) \right], \quad (3.24)$$

$$\frac{\Delta W_0}{N} = -\frac{1}{2} \Delta\gamma \widehat{c}^{(0)}(0) - \frac{1}{2} (1 + \Delta\gamma)^2 \sum_{G \neq 0} |\mu_G|^2 \widehat{c}^{(0)}(G), \quad (3.25)$$

$$\begin{aligned} \frac{\Delta W_b^{(1)}}{N} &= -\frac{1}{2} \rho_l (1 + \Delta\gamma)^2 \sum_G' \sum_{G_2}' \mu_{G_2} \mu_{-G-G_2} \widehat{c}^{(G,1)} \left(\vec{G}_2 + \frac{1}{2} \vec{G} \right), \end{aligned} \quad (3.26)$$

$$\begin{aligned} \frac{\Delta W_b^{(2)}}{N} &= -\frac{1}{2} \rho_l (1 + \Delta\gamma)^2 \sum_G' \sum_{G_2}' \mu_{G_2} \mu_{-G-G_2} \widehat{c}^{(G,2)} \left(\vec{G}_2 + \frac{1}{2} \vec{G} \right), \end{aligned} \quad (3.27)$$

where $\Delta\gamma = (\gamma_s - \gamma_l)/\gamma_l$; the subscripts s and l stand for solid and fluid, respectively. Here ΔW_{id} , ΔW_0 , $\Delta W_b^{(1)}$, and $\Delta W_b^{(2)}$ are, respectively, the ideal, the symmetry-conserving, and the symmetry-broken contributions from the first and second terms of series (2.29) to ΔW . The prime on summation in Eqs. (3.26) and (3.27) indicates the condition $\vec{G} \neq 0$, $\vec{G}_1 \neq 0$, $\vec{G}_2 \neq 0$,

$\vec{G} + \vec{G}_1 \neq 0$, and $\vec{G} + \vec{G}_2 \neq 0$ and

$$\widehat{c}^{(0)}(G) = \int d\vec{r} \overline{c}^{(0)}(r, \gamma_l) e^{i\vec{G} \cdot \vec{r}}, \quad (3.28)$$

$$\widehat{c}^{(G,1)}\left(\vec{G}_2 + \frac{1}{2}\vec{G}\right) = \frac{1}{3} \mu_G \sum_{l_1} \sum_{l_2} \Lambda_1(l_1, l_2, l) Y_{lm}^*(\hat{G}) \int d\vec{r} j_{l_2}\left(\frac{1}{2}Gr\right) \overline{B}_{l_1}(r, G) e^{i(\vec{G}_2 + \frac{1}{2}\vec{G}) \cdot \vec{r}} Y_{lm}(\hat{r}), \quad (3.29)$$

$$\widehat{c}^{(G,2)}\left(\vec{G}_2 + \frac{1}{2}\vec{G}\right) = \widehat{c}^{(G,2,1)}\left(\vec{G}_2 + \frac{1}{2}\vec{G}\right) + 2\widehat{c}^{(G,2,2)}\left(\vec{G}_2 + \frac{1}{2}\vec{G}\right),$$

$$\begin{aligned} \widehat{c}^{(G,2,1)}\left(\vec{G}_2 + \frac{1}{2}\vec{G}\right) &= \frac{1}{6} \sum_{G_1} \mu_{G_1} \mu_K \sum_{lm} \sum_{l'm'} \sum_{l_1 m_1} \sum_{l_2 m_2} \Lambda_{mm'l_1 l_2}^{ll'l_1 l_2} Y_{l'm'}^*(\hat{G}) Y_{l_1 m_1}^*(\hat{G}_1) Y_{l_2 m_2}^*(\hat{K}) \\ &\times \int d\vec{r} j_{l_2}\left(\frac{1}{2}Gr\right) \overline{Q}_{l_1 l_2}(r, G, G_1) e^{i(\vec{G}_2 + \frac{1}{2}\vec{G}) \cdot \vec{r}} Y_{lm}(\hat{r}), \end{aligned} \quad (3.30)$$

$$\begin{aligned} \widehat{c}^{(G,2,2)}\left(\vec{G}_2 + \frac{1}{2}\vec{G}\right) &= \frac{1}{6} \sum_{G_1} \mu_{G_1} \mu_K \sum_{lm} \sum_{l'm'} \sum_{l_1 m_1} \sum_{l_2 m_2} \sum_{l_3 m_3} \Lambda_{mm'l_1 l_2 l_3}^{ll'l_1 l_2 l_3} Y_{l'm'}^*(\hat{G}) Y_{l_2 m_2}^*(\hat{G}_1) Y_{l_3 m_3}^*(\hat{K}) \\ &\times \int d\vec{r} j_{l_2}\left(\frac{1}{2}Gr\right) \overline{N}_{l_1 l_2 l_3}(r, G, G_1) e^{i(\vec{G}_2 + \frac{1}{2}\vec{G}) \cdot \vec{r}} Y_{lm}(\hat{r}). \end{aligned} \quad (3.31)$$

The terms $\frac{\Delta W_0}{N}$, $\frac{\Delta W_b^{(1)}}{N}$, and $\frac{\Delta W_b^{(2)}}{N}$ are, respectively, second, third, and fourth orders in order parameters.

IV. RESULTS FOR FLUID-TO-CRYSTAL TRANSITION

We use the above expression of $\Delta W/N$ to locate the fluid-fcc crystal and the fluid-bcc crystal transitions by varying γ_l , $\Delta\gamma$, and α . For a given γ_l and $\Delta\gamma$, $\Delta W/N$ is minimized with respect to α ; next $\Delta\gamma$ is varied until the lowest value of $\Delta W/N$ at its minimum is found. If this lowest value of $\Delta W/N$ at its minimum is not zero, then γ_l is varied until $\Delta W/N = 0$. The values of the transition parameters, γ_l , $\Delta\gamma$, and α , for a given lattice structure can also be found from simultaneous solution of equations $\frac{\partial}{\partial(\Delta\gamma)}\left(\frac{\Delta W}{N}\right) = 0$, $\frac{\partial}{\partial\alpha}\left(\frac{\Delta W}{N}\right) = 0$, and $\Delta W/N = 0$.

In Table I we compare the values of different terms of $\Delta W/N$ [see Eq. (3.23)] at the freezing point for potentials with $n = 4, 6, 6.5, 7, 12$, and ∞ . The values corresponding to hard spheres are taken from Ref. [14]. The contribution made by the symmetry-broken part to the grand thermodynamic potential at the freezing point is substantial and its importance increases with the softness of the potential. For example, while for $n = \infty$ the contribution of the symmetry-broken part is about 8% of the contribution made by the symmetry-conserved part, it increases to 45% for $n = 4$. As this contribution is negative, it stabilizes the solid phase. Without it the theory strongly overestimates the stability of the fluid phase, especially for softer potentials. This explains why the Ramakrishnan-Yussouff theory gives good results for hard-core potentials but fails for potentials that have a soft-core and/or attractive tail.

The other point to be noted from these results is about the convergence of the series (2.29) which has been used to calculate $c^{(b)}(\vec{r}_1, \vec{r}_2)$. The contribution made by the second

term of the series to the grand thermodynamic potential at the freezing point is found to be negligible compared to that of the first term for $n \geq 6$ and for $n < 6$, though the contribution is small but not negligible. For example, while for $n = 6$ this contribution is about 2% of the first term, for $n = 4$ this increases to 18%. From these results one can conclude that the first two terms of the series of Eq. (2.29) are enough to describe the freezing transition for a wide class of potentials.

In Table II, we compare results of freezing parameters γ_l , γ_s , $\Delta\gamma$, the Lindemann parameter L_n , and $\frac{P\sigma^3}{\epsilon}$, where P is the pressure at the transition point, of the present calculation with those found from computer simulations [21–28] and with the results found by others [12,29–31] using approximate free-energy functionals. The Lindemann parameter is defined as the ratio of the mean-field displacement of a particle to the nearest-neighbor distance in the crystal. For the fcc crystal with the Gaussian density profile of Eq. (3.13) it is given as

$$L_n = \left(\frac{3}{a_{\text{fcc}}^2 \alpha}\right)^{1/2}, \quad (4.1)$$

where $a_{\text{fcc}} = (4/\rho_0)^{1/3}$ is the fcc lattice constant. For the bcc crystal,

$$L_n = \left(\frac{2}{a_{\text{bcc}}^2 \alpha}\right)^{1/2}, \quad (4.2)$$

where $a_{\text{bcc}} = (2/\rho_0)^{1/3}$ is the bcc lattice constant. In Fig. 12 we plot γ_l vs $1/n$ at the transition found from simulations and from the present calculations.

One may note that simulation results have spread (see Table II) and do not agree within each others uncertainties. This may be due to the application of different theoretical

TABLE II. Comparison of the parameters γ_l , γ_s , and $\Delta\gamma$, the Lindemann parameter L , and the pressure P at the coexistence found from different free-energy functional and computer simulations. MWDA denotes the modified weighted density approximation, RY DFT denotes the Ramakrishnan-Yussouff density-functional theory, MHNC denotes the modified hypernetted-chain closure relation, and MSMC denotes the Mayer sampling Monte Carlo.

n	Lattice	Theory/simulation	γ_l	γ_s	$\Delta\gamma$	L	$\frac{P\sigma^3}{\epsilon}$
∞	fcc	Present result	0.937	1.036	0.106	0.09	11.46
		MWDA-static reference [12]	0.863	0.964	0.115	0.13	
		MWDA [12]	0.906	1.044	0.116	0.10	
		RY DFT [29,30]	0.980	1.146	0.174	0.06	
		Simulation [22]	0.939	1.037	0.104	~ 0.13	
		Simulation [23]	0.942	1.041	0.105		
		MC simulation [25]	0.94	1.041	0.107	0.12	11.70
12	fcc	MC simulation [26]	0.939	1.037	0.104		11.57
		Present result	1.17	1.21	0.034	0.11	23.67
		MWDA-static reference [12]	1.12	1.16	0.037	0.14	
		MWDA/MHNC [31]	1.19	1.25	0.046	0.10	
		RY DFT [29]	1.28	1.37	0.07	0.07	
		MC simulation ^a [25]	1.17	1.22	0.042	0.14	23.64
		MSMC technique [27]	1.16	1.20	0.037		23.24
7	fcc	MC simulation [26]	1.16	1.21	0.037		23.41
		Present result	1.84	1.87	0.014	0.12	64.97
		MC simulation ^a [25]	1.85	1.88	0.017	0.15	64.98
	bcc	MC simulation [26]	1.84	1.87	0.016		64.22
		Present result	1.86	1.89	0.015	0.18	67.12
		MC Simulation [26]	1.83	1.86	0.015		63.88
		Present result	2.03	2.06	0.013	0.12	80.11
6.5	fcc	MC simulation ^a [25]	2.04	2.07	0.014	0.15	80.40
		Present result	2.04	2.07	0.014	0.17	78.98
	bcc	MC simulation ^a [28,32]	2.03	2.05	0.010	0.18	78.40
6	fcc	Present result	2.32	2.35	0.012	0.12	103.7
		MWDA-static reference [12]	2.33	2.35	0.007	0.17	
		MWDA/MHNC [31]	2.67	2.72	0.02	0.07	
		RY DFT [29]	3.43	3.52	0.026	0.07	
		MC simulation ^a [25]	2.34	2.37	0.012	0.15	104.5
		MC simulation [26]	2.32	2.35	0.012		103.0
	bcc	Present result	2.30	2.33	0.011	0.16	101.22
		MC simulation ^a [25]	2.32	2.35	0.011	0.17	103.6
		MSMC technique [27]	2.30	2.32	0.011		100.1
		MC simulation [26]	2.30	2.33	0.012		100.0
		MC simulation ^a [28,32]	2.29	2.31	0.009	0.18	99.34
		Present result	5.60	5.63	0.008	0.12	565.6
		MWDA-static reference [12]	5.22	5.26	0.008	0.13	
4	fcc	MWDA/MHNC [31]	8.18	8.24	0.007	0.07	
		RY DFT [29]	12.3	12.47	0.014	0.07	
		MC simulation [25]	5.68	5.71	0.005	0.17	637.0
		Present result	5.57	5.61	0.007	0.16	561.2
	bcc	MWDA-static reference [12]	5.05	5.09	0.008	0.18	
		MC simulation [25]	5.73	5.75	0.004	0.18	648.0

^aIndicates values obtained from interpolation of the tabulated values.

methods used in locating the transition and system sizes in the calculations. The other sources of errors include the existence of an interface, truncation of the potential, free-energy bias, and so on. Agrawal and Kofke [25], who have reported results for $0 \leq 1/n \leq 0.33$, have considered a system of 500 particles only. Since they have not used finite-size corrections, their results for softer potentials (say $n \lesssim 6$) may not be accurate. For example, they reported that for $1/n > 0.16$ fluid freezes into a bcc structure but for $1/n = 0.25$ they found that the γ_l for the fluid-bcc transition is higher than that of the fluid-fcc

transition. The recent calculations where large systems have been considered [26–28] results are available for $n \geq 5$ (or $1/n < 0.2$). From these results it is found that fluid freezes into fcc crystal for $n \geq 7$ and for $n < 7$ the bcc structure is preferred; the fluid-bcc-fcc triple point is estimated to be close to $1/n \sim 0.15$.

From Table II and Fig. 12 we find that our results are in very good agreement with simulation results for all cases. We find that for $n > 6.5$ the fluid freezes into a fcc structure while for $n \leq 6$ it freezes into a bcc structure. The fluid-bcc-fcc triple

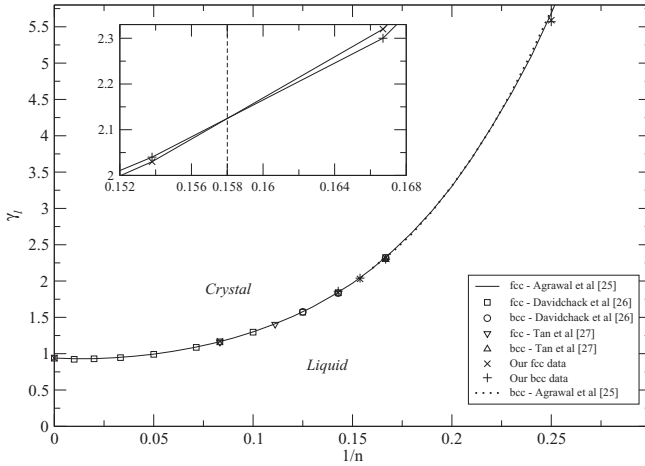


FIG. 12. Comparison of equilibrium phase diagram of $\frac{1}{n}$ vs γ_l found from simulation results and from our theory. In inset the fluid-fcc and fluid-bcc transition lines are plotted at a magnified scale and the fluid-bcc-fcc triple point is found at $\frac{1}{n} = 0.158$.

point is found at $\frac{1}{n} = 0.158$ (see the inset in Fig. 12). The value of Lindemann parameter found by us is, however, somewhat lower than those found by Agrawal and Kofke [25] and Saija *et al.* [32]. The energy difference between the two cubic structures at the transition is found to be small in agreement with the simulation results [28].

V. SUMMARY AND PERSPECTIVES

We used a free-energy functional for a crystal proposed by Singh and Singh [13] to investigate the crystallization of fluids interacting via power-law potentials. This free-energy functional was found by performing double functional integration in the density space of a relation that relates the second functional derivative of $A[\rho]$ with respect to $\rho(\vec{r})$ to the DPCF of the crystal. The expression found for $A[\rho]$ is exact and contains both the symmetry-conserved part of the DPCF, $c^{(0)}(r, \rho)$, and the symmetry-broken part, $c^{(b)}(\vec{r}_1, \vec{r}_2)$. The symmetry-conserved part corresponds to the isotropy and homogeneity of the phase and passes smoothly to the frozen phase at the freezing point, whereas the symmetry-broken part arises due to heterogeneity which sets in at the freezing point and vanishes in the fluid phase. The values of $c^{(0)}(r)$ and its derivatives with respect to density ρ as a function of interparticle separation r have been determined using an integral equation theory comprising the OZ equation and the closer relation of Roger and Young [20]. From the results of $\frac{\partial c^{(0)}(r)}{\partial \rho}$ and $\frac{\partial^2 c^{(0)}(r)}{\partial \rho^2}$, we calculated the three- and four-body direct correlation functions of the isotropic phase. These results have been used in a series written in ascending powers of the order parameters to calculate $c^{(b)}(\vec{r}_1, \vec{r}_2)$. The contributions made by the first and second terms of the series have been calculated for bcc and fcc crystals. The contribution made by the second term is found to be considerably smaller than the first term, indicating that the first two terms are enough to give accurate values for $c^{(b)}(\vec{r}_1, \vec{r}_2)$. The values of $c^{(G)}(\vec{r})$ for bcc and fcc structures are found to differ considerably.

The contribution of the symmetry-broken part of DPCF to the free energy is found to depend on the nature of pair potentials; the contribution increases with softness of potentials. In the case of power-law potentials we found that the contribution to the grand thermodynamic potential at the freezing point arising from the second term of the series (2.29) which involves four-body direct correlation function is negligible for $n > 6$ and small but not negligible for $n < 6$. For $n = 4$ the contribution made by the second term is about 18% of the first term. The contribution made by the second term is positive, whereas the contribution of the first term is negative. As the net contribution made by the symmetry-broken term is negative, it stabilizes the solid phase. Without the inclusion of this term the theory strongly overestimates the stability of the fluid phase, especially for softer potentials. Our results reported in this paper and elsewhere [14,17] explain why the Ramakrishnan-Yussouff theory gives good results for hard-core potentials but fails for potentials that have a soft-core/or attractive tail.

The agreement between theory and simulation values of freezing parameters found for potentials with n varying from 4 to ∞ indicates that the free-energy functional used here with values of $c^{(b)}(\vec{r}_1, \vec{r}_2)$ calculated from the first two terms of the series (2.29) provides an accurate theory for freezing transitions for a wide class of potentials. Since this free-energy functional takes into account the spontaneous symmetry breaking, it can be used to study various phenomena of ordered phases near their melting points.

ACKNOWLEDGMENT

A.S.B. thanks the University Grants Commission (New Delhi, India) for the research grant.

APPENDIX

In this Appendix we calculate $c_3^{(0)}(\vec{r}_1, \vec{r}_2, \vec{r}_3)$ and $c_4^{(0)}(\vec{r}_1, \vec{r}_2, \vec{r}_3, \vec{r}_4)$. Using the notation $r = |\vec{r}_2 - \vec{r}_1|$, $r' = |\vec{r}_3 - \vec{r}_1|$, and $|\vec{r}' - \vec{r}| = |\vec{r}_3 - \vec{r}_2|$ we write $c_3^{(0)}(\vec{r}_1, \vec{r}_2, \vec{r}_3)$ as [see Eq. (2.23)]

$$c_3^{(0)}(\vec{r}, \vec{r}') = t(r)t(r')t(|\vec{r}' - \vec{r}|). \quad (\text{A1})$$

The function $t(|\vec{r}' - \vec{r}|)$ can be expanded in spherical harmonics,

$$t(|\vec{r}' - \vec{r}|) = \frac{2}{\pi} \sum_{lm} A_l(r, r') Y_{lm}(\hat{r}) Y_{lm}^*(\hat{r}'), \quad (\text{A2})$$

where

$$A_l(r, r') = \int_0^\infty dq q^2 t(q) j_l(qr) j_l(qr'). \quad (\text{A3})$$

Here $j_l(x)$ is the spherical Bessel function and $Y_{lm}(\hat{r})$ the spherical harmonics.

From Eqs. (A1) and (A2) we get

$$c_3^{(0)}(\vec{r}, \vec{r}') = \frac{2}{\pi} \sum_{lm} D_l(r, r') Y_{lm}(\hat{r}) Y_{lm}^*(\hat{r}'), \quad (\text{A4})$$

where

$$D_l(r, r') = A_l(r, r') t(r) t(r').$$

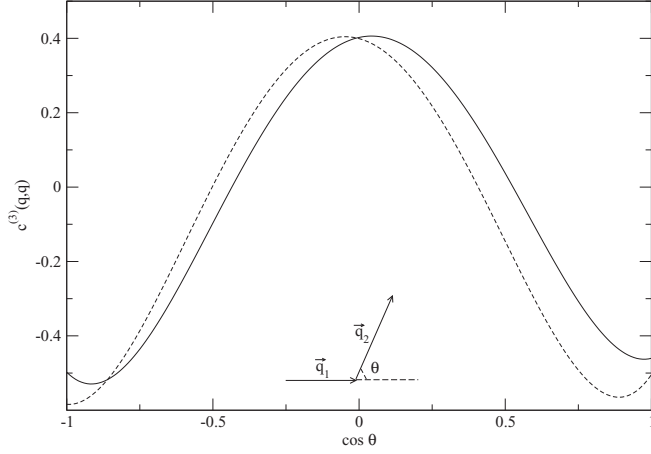


FIG. 13. Values of $\hat{c}_3^{(0)}(q, q, q)$ as a function of $\cos\theta$ (geometry is shown schematically in the figure) for $q_1 a_0 = q_2 a_0 = 4.3$ and for potentials $n = 12, \gamma_l = 1.17$ (dashed curve) and $n = 6, \gamma_l = 2.30$ (full curve).

The Fourier transform of Eq. (A4), defined as

$$\hat{c}_3^{(0)}(\vec{q}_1, \vec{q}_2) = \rho^2 \int d\vec{r} \int d\vec{r}' e^{-i\vec{q}_1 \cdot \vec{r}} e^{-i\vec{q}_2 \cdot \vec{r}'} c_3^{(0)}(\vec{r}, \vec{r}'),$$

gives

$$\hat{c}_3^{(0)}(\vec{q}_1, \vec{q}_2) = 32\pi \sum_{lm} (-1)^l D_l(q_1, q_2) Y_{lm}(\hat{q}_1) Y_{lm}^*(\hat{q}_2), \quad (\text{A5})$$

where

$$D_l(q_1, q_2) = \rho^2 \int dr r^2 \int dr' r'^2 j_l(q_1 r) j_l(q_2 r') D_l(r, r'). \quad (\text{A6})$$

The value of $\hat{c}_3^{(0)}(\vec{q}_1, \vec{q}_2)$ is plotted in Fig. 13 for $q_1 = q_2 = q_{\max}$ for various angles θ such that $0 < |\vec{q}_1 + \vec{q}_2| < 2q_{\max}$, where θ is the angle between \vec{q}_1 and \vec{q}_2 as shown in the figure. The values plotted in this figure correspond to $q a_0 = 4.3$ and for $n = 6, \gamma_l = 2.30$ (full line) and $n = 12, \gamma_l = 1.17$ (dashed line). In Fig. 14 we plot values of $\hat{c}_3^{(0)}(\vec{q}_1, \vec{q}_2)$ for an equilateral triangle with various side lengths. The values for $n = 12, \gamma_l = 1.17$ are in good agreement with the values given in Ref. [6] (see Figs. 3 and 4 of Ref. [6]).

For $c_4^{(0)}(\vec{r}_1, \vec{r}_2, \vec{r}_3, \vec{r}_4)$ the contribution arises from three diagrams shown in Eq. (2.28). Using the notation $|\vec{r}_4 - \vec{r}_1| = r''$, $|\vec{r}_4 - \vec{r}_2| = |\vec{r}'' - \vec{r}|$, $|\vec{r}_4 - \vec{r}_3| = |\vec{r}'' - \vec{r}'|$ and other notations defined above we get

$$c_4^{(0)}(\vec{r}, \vec{r}', \vec{r}'') = \begin{array}{c} \text{Diagram 1} \\ + \\ \text{Diagram 2} \\ + \\ \text{Diagram 3} \end{array}, \quad (\text{A7})$$

Each diagram of Eq. (A7) has two circles connected by three bonds, two s bonds (dashed line) and one t bond (full line), where one of the remaining circles is connected by two t bonds and the other by two s bonds. By permuting circles one can convert one diagram into another. The values of $c_4^{(0)}(\vec{r}, \vec{r}', \vec{r}'')$ depend on three vectors, \vec{r} , \vec{r}' , and \vec{r}'' .

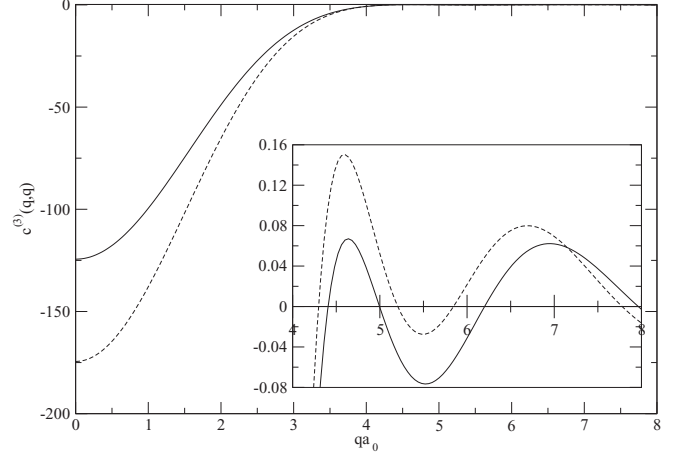


FIG. 14. Values of $\hat{c}_3^{(0)}(q, q, q)$ vs $q a_0$ (equilateral triangles). The dashed curve represents the values for $n = 12, \gamma_l = 1.17$ and full curve for $n = 6, \gamma_l = 2.30$. Inset shows values for $q a_0 \geq 4.0$ on magnified scale.

We calculate $\hat{c}_4^{(0)}(\vec{q}_1, \vec{q}_2, \vec{q}_3)$ defined as

$$\hat{c}_4^{(0)}(\vec{q}_1, \vec{q}_2, \vec{q}_3) = \rho^3 \int d\vec{r} \int d\vec{r}' \times \int d\vec{r}'' e^{-i\vec{q}_1 \cdot \vec{r}} e^{-i\vec{q}_2 \cdot \vec{r}'} e^{-i\vec{q}_3 \cdot \vec{r}''} c_4^{(0)}(\vec{r}, \vec{r}', \vec{r}''), \quad (\text{A8})$$

Using Eq. (A7) and writing each diagram in terms of t and s bonds we get

$$\begin{aligned} \hat{c}_4^{(0)}(\vec{q}_1, \vec{q}_2, \vec{q}_3) &= \frac{108}{\pi^2} \sum_{l_1 m_1} \sum_{l_2 m_2} \sum_{l_3 m_3} (-i)^{(l_1 + l_2 + l_3)} \Lambda_{l_1 l_2 l_3}^{m_1 m_2 m_3} M_{l_1 l_2 l_3}(q_1, q_2, q_3) \\ &\times [Y_{l_3 m_3}^*(\hat{q}_1) Y_{l_1 m_1}(\hat{q}_2) Y_{l_2 m_2}(\hat{q}_3) \\ &+ Y_{l_1 m_1}(\hat{q}_1) Y_{l_3 m_3}^*(\hat{q}_2) Y_{l_2 m_2}(\hat{q}_3) \\ &+ (-1)^{l_1} Y_{l_1 m_1}(\hat{q}_1) Y_{l_3 m_3}^*(\hat{q}_2) Y_{l_2 m_2}(\hat{q}_3)], \end{aligned} \quad (\text{A9})$$

where

$$\Lambda_{l_1 l_2 l_3}^{m_1 m_2 m_3} = \left[\frac{(2l_1 + 1)(2l_2 + 1)}{4\pi(2l_3 + 1)} \right]^{1/2} C_g(l_1, l_2, l_3; 0, 0, 0) \times C_g(l_1, l_2, l_3; m_1, m_2, m_3) \quad (\text{A10})$$

and

$$\begin{aligned} M_{l_1 l_2 l_3}(q_1, q_2, q_3) &= \rho^3 \int_0^\infty dr r^2 s(r) \int_0^\infty d\vec{r}' r'^2 t(r') \int_0^\infty d\vec{r}'' r''^2 s(r'') \\ &\times j_{l_1}(q_1 r) j_{l_2}(q_2 r') j_{l_3}(q_3 r'') A_{l_1}(r, r') E_{l_2}(r, r''). \end{aligned} \quad (\text{A11})$$

$A_{l_1}(r, r')$ is defined by Eq. (A3). $E_{l_2}(r, r'')$ is given as

$$E_{l_2}(r, r'') = \int_0^\infty dq q^2 s(q) j_l(qr) j_l(qr''). \quad (\text{A12})$$

The values of $\hat{c}_4^{(0)}(\vec{q}_1, \vec{q}_2, \vec{q}_3)$ depend on magnitudes and directions of vectors \vec{q}_1 , \vec{q}_2 , and \vec{q}_3 . In Figs. 15 and 16 we

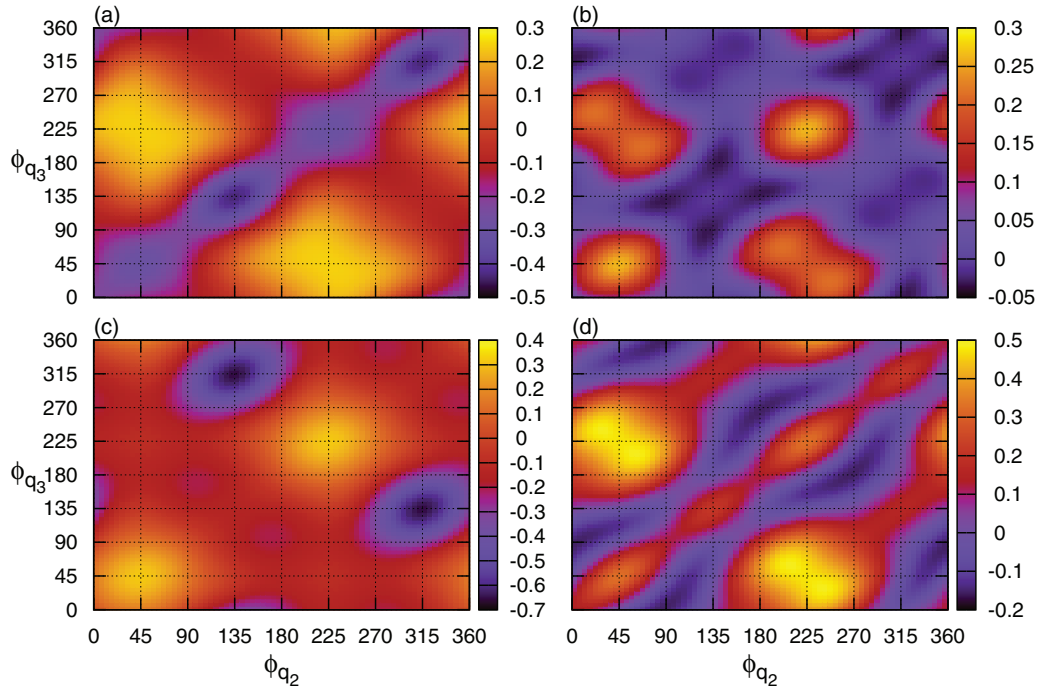


FIG. 15. (Color online) Values of $\hat{c}_4^{(0)}(\vec{q}_1, \vec{q}_2, \vec{q}_3)$ (shown using a color code shown on the right-hand side of each figure) as a function of ϕ_{q_2} and ϕ_{q_3} for $q_1 = q_2 = q_{\max}$ with $q_{\max}a_0 = 4.3$, $\theta_{q_1} = 0^\circ$, $\phi_{q_1} = 0^\circ$: (a) $\theta_{q_2} = 45^\circ$, $\theta_{q_3} = 45^\circ$, (b) $\theta_{q_2} = 45^\circ$, $\theta_{q_3} = 90^\circ$, (c) $\theta_{q_2} = 90^\circ$, $\theta_{q_3} = 45^\circ$, and (d) $\theta_{q_2} = 90^\circ$, $\theta_{q_3} = 90^\circ$.

use color codes (shown at the right-hand side of each figure) to plot values of $\hat{c}_4^{(0)}(\vec{q}_1, \vec{q}_2, \vec{q}_3)$ for $q_1 = q_2 = q_3 = q_{\max}$ as a function of ϕ_{q_2} and ϕ_{q_3} for different choices of θ_{q_2} and θ_{q_3} . The values of $q_{\max}a_0$ is taken to be equal to 4.3 as in Fig. 13. While the values plotted in Fig. 15 correspond to $\theta_{q_1} = 0^\circ$, the

values plotted in Fig. 16 correspond to $\theta_{q_1} = 90^\circ$ and $\phi_{q_1} = 0^\circ$. These figures show how the values of $\hat{c}_4^{(0)}(\vec{q}_1, \vec{q}_2, \vec{q}_3)$ depend on orientations of vectors \vec{q}_1 , \vec{q}_2 , and \vec{q}_3 . Emergence of ordering in maxima and minima depending on orientations of these vectors is evident.

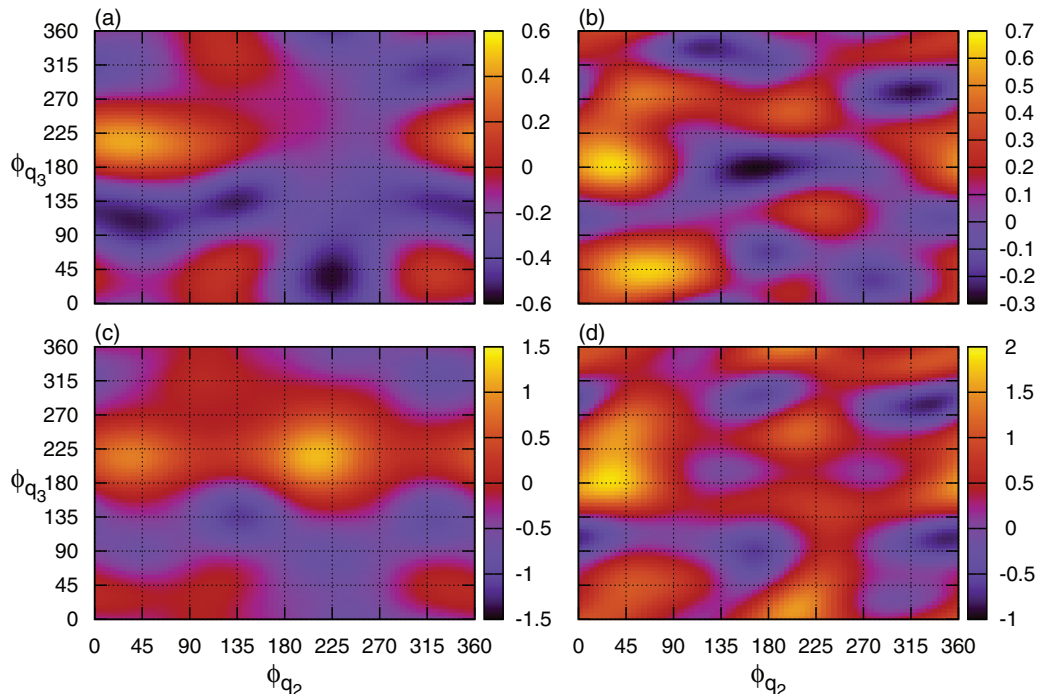


FIG. 16. (Color online) Same as described in the in caption to Fig. 15 except for $\theta_{q_1} = 90^\circ$ and $\phi_{q_1} = 0^\circ$.

- [1] J. G. Kirkwood and E. Monroc, *J. Chem. Phys.* **9**, 514 (1951).
- [2] Y. Singh, *Phys. Rep.* **207**, 351 (1991).
- [3] H. Lowen, *Phys. Rep.* **237**, 249 (1994).
- [4] T. V. Ramakrishnan and M. Yussouff, *Phys. Rev. B* **19**, 2775 (1979).
- [5] A. D. J. Haymet and D. W. Oxtoby, *J. Chem. Phys.* **74**, 2559 (1981).
- [6] J. L. Barrat, J. P. Hansen, and G. Pastore, *Mol. Phys.* **63**, 747 (1988); *Phys. Rev. Lett.* **58**, 2075 (1987).
- [7] W. A. Curtin, *J. Chem. Phys.* **88**, 7050 (1988).
- [8] P. Tarazona, *Phys. Rev. A* **31**, 2672 (1985).
- [9] W. A. Curtin and N. W. Ashcroft, *Phys. Rev. A* **32**, 2909 (1985).
- [10] A. R. Denton and N. W. Ashcroft, *Phys. Rev. A* **39**, 4701 (1989).
- [11] C. N. Likos and N. W. Ashcroft, *J. Chem. Phys.* **99**, 9090 (1993).
- [12] D. C. Wang and A. P. Gast, *J. Chem. Phys.* **110**, 2522 (1999).
- [13] S. L. Singh and Y. Singh, *Europhys. Lett.* **88**, 16005 (2009).
- [14] S. L. Singh, A. S. Bharadwaj, and Y. Singh, *Phys. Rev. E* **83**, 051506 (2011).
- [15] J. P. Hansen and I. R. McDonald, *Theory of Simple Liquids*, 3rd ed. (Academic Press, Boston, 2006).
- [16] P. Mishra and Y. Singh, *Phys. Rev. Lett.* **97**, 177801 (2006); P. Mishra, S. L. Singh, J. Ram, and Y. Singh, *J. Chem. Phys.* **127**, 044905 (2007).
- [17] A. Jaiswal, S. L. Singh, and Y. Singh, *Phys. Rev. E* **87**, 012309 (2013).
- [18] J. S. McCarley and N. W. Ashcroft, *Phys. Rev. E* **55**, 4990 (1997).
- [19] A. Jaiswal and Y. Singh (unpublished).
- [20] F. J. Rogers and D. A. Young, *Phys. Rev. A* **30**, 999 (1984).
- [21] W. G. Hoover, M. Ross, K. W. Johnson, D. Henderson, J. A. Barker, and B. C. Brown, *J. Chem. Phys.* **52**, 4931 (1970).
- [22] W. G. Hoover and F. H. Ree, *J. Chem. Phys.* **49**, 3609 (1968).
- [23] B. J. Alder, W. G. Hoover, and D. A. Young, *J. Chem. Phys.* **49**, 3688 (1968).
- [24] H. Ogura, H. Matsuda, T. Ogawa, N. Ogita, and A. Veda, *Prog. Theor. Phys.* **58**, 419 (1992).
- [25] R. Agrawal and D. A. Kofke, *Mol. Phys.* **85**, 23 (1995).
- [26] R. L. Davidchack and B. B. Laird, *Phys. Rev. Lett.* **94**, 086102 (2005).
- [27] T. B. Tan, A. J. Schultz, and D. A. Kofke, *Mol. Phys.* **109**, 123 (2011).
- [28] S. Prestipino, F. Saija, and P. V. Giaquinta, *J. Chem. Phys.* **123**, 144110 (2005).
- [29] J. L. Barrat, J. P. Hansen, G. Pastore, and E. M. Waisman, *J. Chem. Phys.* **86**, 6360 (1987).
- [30] B. B. Laird, J. D. McCoy, and A. D. J. Heymat, *J. Chem. Phys.* **87**, 5449 (1987).
- [31] B. B. Laird and D. M. Kroll, *Phys. Rev. A* **42**, 4810 (1990).
- [32] F. Saija, S. Prestipino, and P. V. Giaquinta, *J. Chem. Phys.* **124**, 244504 (2006).